NASA TECHNICAL MEMORANDUM

NASA TM X-1739

NASA TM X-1739

CASE FILE COPY

PERFORMANCE CHARACTERISTICS FROM MACH 2.58 TO 1.98 OF AN AXISYMMETRIC MIXED-COMPRESSION INLET SYSTEM WITH 60-PERCENT INTERNAL CONTRACTION

by Robert W. Cubbison, Edward T. Meleason, and David F. Johnson

Lewis Research Center
Cleveland, Ohio

NATIONAL AERONAUTICS AND SPACE ADMINISTRATION • WASHINGTON, D. C. • FEBRUARY 1969

NASA TM X-1739

PERFORMANCE CHARACTERISTICS FROM MACH 2.58 TO 1.98 OF AN AXISYMMETRIC MIXED-COMPRESSION INLET SYSTEM WITH 60-PERCENT INTERNAL CONTRACTION

By Robert W. Cubbison, Edward T. Meleason, and David F. Johnson

Lewis Research Center
Cleveland, Ohio

NATIONAL AERONAUTICS AND SPACE ADMINISTRATION

For sale by the Clearinghouse for Federal Scientific and Technical Information
Springfield, Virginia 22151 – CFSTI price $3.00

ABSTRACT

A study has been made in the Lewis 10- by 10-Foot Supersonic Wind Tunnel to determine the performance characteristics of an axisymmetric, mixed-compression inlet system designed for Mach 2.5. Inlet performance is presented for 0° and maximum unstart angle of attack. Diffuser static-pressure distributions and compressor face total-pressure profiles are shown for several operating conditions. Data presented show effects of Mach number, Reynolds number, bypass flow, and vortex generators on performance. Performance during restart cycles and required area ratios for restart are presented.

PERFORMANCE CHARACTERISTICS FROM MACH 2.58 TO 1.98 OF AN AXISYMMETRIC MIXED-COMPRESSION INLET SYSTEM WITH 60-PERCENT INTERNAL CONTRACTION

by Robert W. Cubbison, Edward T. Meleason, and David F. Johnson

Lewis Research Center

SUMMARY

A study had been made to determine the performance characteristics of an axisymmetric, mixed-compression inlet system designed for Mach 2.5. Sixty percent of the overall supersonic area contraction occurred internally. The spike could be translated to vary the internal contraction ratio. The inlet also included a high-response overboard bypass system for shock-position control and a low-speed valve to control secondary flow through the nacelle for cooling purposes.

Data were obtained over the nominal Mach range of 2.0 to 2.6 for angles of attack of 0° and the maximum value prior to an unstart. The Reynolds number varied from 1.24×10^{6} to 3.82×10^{6} based on the inlet cowl-lip diameter.

A moderate stable operating range between design airflow conditions and inlet unstart was obtained at zero angle of attack for all Mach numbers without large sacrifices in performance. At Mach 2.5, this range was about 10.5 percent of design corrected airflow. At maximum angle of attack of about 2.7°, this range was sizeably reduced. The overall pressure recovery level of the inlet increased, and the distortion decreased at all Mach numbers as bypass flow increased up to about 12.5 percent of the capture flow rate. Installing vortex generators on the centerbody prevented flow separation from the centerbody for bypass flows up to 40 percent of capture. Without generators, separation occurred at bypass flow rates above about 12.5 percent. For the airflow schedule assumed, the pressure recovery increased about 1.6 percent as the Mach number was reduced from 2.5 to 2.3 and then decreased about 2.2 percent when the Mach number was reduced to 2.0. Above Mach 2.5, the recovery decreased rapidly. Reducing the Reynolds number from 3.82×10^{6} to 1.24×10^{6} at Mach 2.5 reduced the maximum pressure recovery for maximum engine mass flow ratio by about 3 percent. The corresponding distortion level increased from 0.102 to 0.167.

INTRODUCTION

To date, very little information has been published about the inlet-engine dynamics of a complete airbreathing propulsion system operating at supersonic speeds. In order to investigate this area and the associated control problems, an experimental program is being conducted in the Lewis 10- by 10-Foot Supersonic Wind Tunnel. For the initial tests, an axisymmetric inlet was selected with a design Mach number of 2.5 and with 60 percent of the supersonic area contraction occurring internally. The results from a previous investigation to determine the effect of the amount and the location of porous bleed on the performance of this inlet are reported in reference 1. Further work on the effect of bleed-system backpressure on the overall inlet performance is presented in reference 2. The present report presents the results obtained with a choked exit plug to determine the overall performance characteristics of this inlet with operating bypasses prior to its use with a turbojet engine.

In an efficient propulsion system, a high level of performance is required from all of the components. For example, the inlet must provide the correct amount of high recovery flow with low distortion to the engine. The necessary boundary-layer bleed pattern for high recovery was based on the results of reference 1. With the engine installed, it is also necessary to provide bypass flow capability for terminal-shock-position control and for engine and nozzle cooling. In the present system, both a high-response overboard bypass for shock control and a slow-acting bypass for engine cooling were provided.

Performance maps showing variations of both engine speed (simulated with a choked-exit plug) and overboard bypass are presented. Diffuser static-pressure distributions, compressor-face total-pressure profiles, and inlet restart maps are included. Data are also shown on the effects of Mach number, angle of attack, bypass flow, vortex generators, and Reynolds number.

The test was conducted at Mach numbers of 1.98 to 2.58 at zero angle of attack and at maximum angle of attack before inlet unstart. Free-stream total temperature was varied from 317 to 400 K and Reynolds number based on inlet capture diameter was varied from 1.24 to 3.82×10^6.

SYMBOLS

A	flow area
A_c	capture area, 0.1758 m^2
A_{cowl}	flow area at cowl lip station bounded by model geometry
b	vortex generator height, 1.27 cm

D_c	cowl lip diameter, 0.4732 m
d	distance
H	annulus height at diffuser station 5
h	distance from centerbody surface
M	Mach number
m/m_0	mass-flow ratio
N	engine speed
N^*	rated engine speed, 16 500 rpm
P	total pressure
p	static pressure
R_c	cowl-lip radius, 0.2366 m
Re	Reynolds number
r	radius
T	total temperature
$W\sqrt{\theta}/\delta$	engine corrected airflow
x	axial distance from spike tip
α	angle of attack
δ	$P/10.131\times10^3$ N/m^2
θ	T/288.2 K
θ_l	cowl-lip-position parameter, $\tan^{-1} 1/(x/R_c)$

Subscripts:

av	average
bl	bleed
by	bypass
capt	capture
ej	ejector
h	local conditions along rake
l	lip
max	maximum

min	minimum
x	local
0	free stream
5	diffuser exit

APPARATUS AND PROCEDURE

The inlet used in this investigation was an axisymmetric mixed-compression type designed for Mach 2.5 with a translating centerbody for inlet start and off-design operation. At design Mach number, 40 percent of the supersonic flow area contraction was external and 60 percent was internal. The inlet was attached to a nacelle in which either a J-85/13 turbojet engine or a choked-exit plug assembly could be installed. For this study, only the choked-plug assembly was used. Figure 1 is a photograph of the inlet-nacelle combination mounted from a vertical strut in the wind-tunnel test section. The bulge in the nacelle was required to house the engine accessory package.

The engine match corrected airflow requirement was 15.83 kilograms per second at a temperature of 390 K. Based on an inlet pressure recovery of 0.90 at the design Mach number of 2.5 (ref. 1), it was determined that the capture airflow would be distributed as follows: 88.6 percent for the engine, 5.5 percent for the throat bleed system to increase inlet performance, 4.0 percent for engine cooling, and 1.9 percent for the overboard bypass to provide a margin for shock position control. The assumed engine corrected airflow schedule over the test Mach range is shown in figure 2.

Some elements of the inlet aerodynamic design are presented in figure 3. External compression was accomplished with a 12.5° half-angle conical centerbody. Internally, the initial cowl-lip angle of 0° generated a shock that reflected twice before reaching the throat. In addition, isentropic compression was also included. The theoretical average supersonic throat Mach number was 1.239 with a supersonic total-pressure recovery of 0.988. Internal contours and flow conditions in the supersonic diffuser were calculated with the aid of reference 3. The subsonic diffuser consisted of an initial throat region four hydraulic radii in length with a 1° equivalent conical expansion followed by the main diffuser that was designed as an 8° equivalent conical expansion. The subsonic diffuser length using these criteria would be 3.5 cowl-lip radii. However, additional length of essentially constant area was provided to accommodate the bypass system. The resulting overall design length from cone tip to compressor face was 7.72 cowl-lip radii. Figure 3(b) shows the internal area distribution for several spike positions. A more complete discussion on the aerodynamic design of the inlet is contained in reference 1.

Provisions were also included for installing vortex generators on the cowl and cen-

terbody just aft of the throat region at 0.980 meter downstream of the design spike tip position. Details of the various generator configurations are shown in figure 4. The basic generator shape was derived from the NACA 0012 airfoil. In one case (fig. 4(a)) the basic ordinates were used for the upper surface and the original airfoil mean-camber line formed the lower surface. The radius of the leading-edge circle was 0.0154 centimeter. For the other configuration, the complete NACA 0012 airfoil was used. The generator height (1.27 cm) was selected to be about equal to the local boundary-layer height. With a chosen aspect ratio of 0.5, the required chord length was 2.54 centimeters. The angle of attack of successive generators relative to the local flow was alternately plus and minus 16°. This installation results in the converging (C) and diverging (D) pair orientation shown in figure 4. In general, two different vortex generator spacings were tested: a narrow space (N) of approximately three generator heights (fig. 4(a)) and a wide space (W) of about six heights (fig. 4(b)). The small difference in the spacings between cowl and centerbody generators indicated in the figure is a result of requiring an equal number of converging and diverging pairs on the respective surfaces. Two orientations of generator pairs (relative to the centerbody support struts) were studied for their effect on the quality of flow along the strut surfaces. Configurations NC and WC had a converging pair ahead of the struts, ND and WD a diverging pair.

Details of the model configurations used in this investigation are shown in figure 5. An isometric view of the inlet is shown in figure 5(a). The bleed patterns (fig. 5(b)) were selected on the basis of the results presented in reference 1. Configuration I (no throat bleed) is identical to configuration A of that reference. This pattern was found to be the most efficient from a payload viewpoint. However, a small change in diffuser back pressure would cause the terminal shock to move completely through the throat region. To study the duct dynamics and inlet-engine interactions, it is desirable that a small disturbance produce a well-defined shock movement. Bleed in the throat region will reduce the extent the shock moves for a small change in back pressure. As a result, configuration II was derived from configuration I by adding the throat bleed indicated in figure 5(b). This bleed was positioned at about the location of the leading edge of the terminal shock train during normal operation at design Mach number.

The bleed flows from all regions were discharged overboard. Both cowl bleed flows were discharged through exits shown in figure 5(c) which have a 15° discharge angle relative to the external surface. These exits were sufficiently large to ensure choking of the porous surface. The fore and aft centerbody bleed flows were combined into one plenum and ducted through the upper two centerbody support struts to 30° louvered exits on the cylindrical portion of the nacelle. The bottom strut exit was sealed because the nacelle bulge (fig. 1) covered about two-thirds of the opening and the pressure rise due to this bulge may have unchoked this exit. The exit areas of the remaining two struts were large enough to ensure choking of the bleed holes.

The inlet design included two remotely controlled flow bypass systems: a high response overboard system for shock position control, and a low-speed valve to control secondary flow through the nacelle for engine and ejector cooling. Details of the bypass plenum entrance are shown in figure 5(c). The entrance slot to the plenum was sized to pass 94.5 percent of the capture mass flow at the design Mach number assuming a total pressure at the slot entrance equal to the main duct (or compressor face) static pressure. Based on the air management schedule, the flow would then be discharged overboard through 45° louvered door units (fig. 5(c) and (d)) and also through the ejector valve openings into the nacelle (fig. 5(c) and (e)). The overboard bypass exit area was sized to remove 88 percent of the on-design capture mass flow assuming again that main-duct static pressure equals the total pressure ahead of the choked bypass exit. The remaining flow (6.5 percent of capture) would be discharged through the ejector valve. However, the design capability of this valve was 10 percent of capture mass flow assuming main-duct static pressure at the entrance of the choked valve. Both the bypass entrance and plenum were divided into six separate sections by the centerbody support struts and cowl ribs. To ensure uniform flow removal, six overboard door units (one per section) were symmetrically located around the periphery of the bypass plenum. An equal number of ejector valve openings were similarly located in the base of the bypass plenum. Besides the steady-state mode of operation used in the present study, the overboard bypass system could be operated sinusoidally at frequencies up to 140 hertz with a flat amplitude response of 0.254 centimeter peak-to-peak at frequencies up to 100 hertz.

The overall inlet total-pressure recovery just ahead of the compressor face was determined from rakes 1 to 6 (fig. 5(f)) which were area weighted. Additional measurements (rakes 7 to 10) were included in the distortion calculations and in plots of the total-pressure profiles. Static-pressure distributions along the top centerline of both cowl and centerbody were also measured.

The diffuser exit or engine mass-flow ratio was calculated using a calibrated choked plug and an average of eight static pressures in the cold pipe located 4.3 cowl-lip radii ahead of the plug exit. Cowl bleed flow rates at both stations were determined from a measured static and total pressure at their respective exits (see fig. 5(c)) and the measured exit areas. Flow from the combined centerbody bleed regions was calculated from the pitot-static measurements that were taken by the rake in the centerbody cavity just ahead of the support struts. Ejector bypass mass-flow ratio was calculated from the sonic flow relation using the measured bypass plenum total pressure (see fig. 5(c)), the measured valve opening, and experimentally determined flow coefficients. The overboard bypass mass-flow ratio at 0° angle of attack was then determined by subtracting the sum of the engine, ejector bypass, and the three bleed mass-flow ratios from the theoretical capture mass-flow ratio for the spike position and Mach number in question.

The test was conducted in the Lewis 10- by 10-Foot Supersonic Wind Tunnel from

Mach 2.58 to 1.98 at zero angle of attack and at maximum angle before unstart. The Reynolds number based on inlet cowl-lip diameter varied from 1.24 to 3.82×10^6. Free-stream total temperature was varied from 317 to 400 K. Temperature levels above the normal tunnel operating levels were obtained using the natural gas fired heater installed in the tunnel bellmouth upstream of the supersonic nozzle. On the aerodynamic cycle (normally used for isolated inlet testing without heat addition) the normal temperature levels are 317 K for Mach 2.0 to 2.5 and 372 K for Mach 2.5 to 2.6. The 55 K step change at Mach 2.5 results from the startup of the second tunnel compressor, which is required for tunnel operation above Mach 2.5. For the propulsion cycle (used for engine tests, tunnel heater operation, or both) the normal unheated levels at all Mach numbers are reduced about 25 K. A potential disadvantage of using a gas-fired heater installed in the stream is the possibility of flow nonuniformities resulting from condensation of the water vapor that is introduced into the flow. It was found in reference 4 that in the 10- by 10-Foot Supersonic Wind Tunnel the test section Mach number and total pressure were decreased by this effect. For example, at Mach 2.5 the temperature rise from 317 to 373 K results in a Mach number reduction from 2.50 to 2.47. At Mach 2.3, the temperature increment of 68 K reduced Mach number by 0.063, and at Mach 2.0, the Mach number decrement was 0.032 from a temperature increase of 30 K. As discussed in reference 4, these changes in flow conditions were repeatable and were accurately calibrated. Of primary interest in the present study is this Mach reduction that could influence the inlet performance. The optimum inlet geometry (spike position) was determined for the unheated test condition. This geometry was held fixed for both the heated and unheated conditions. At the nominal Mach 2.3 test condition, the optimum inlet configuration corresponded to a near-maximum contraction ratio and, as a result, the Mach number reduction due to heater operation was sufficient to unstart the inlet. Consequently, the tunnel wall was positioned at the next higher nominal setting (M = 2.4) prior to the addition of heat. The resulting free-stream Mach number was 2.34.

RESULTS AND DISCUSSION

Throughout the following discussion, the nominal value of Mach number will generally be used. The actual free-stream values are indicated in the figures and when used in the text will be referred to as the free-stream Mach number.

The general presentation of the basic performance data of the inlet system is as follows: (1) mass-flow ratio, total-pressure recovery, and distortion characteristics in figures 6 and 7; (2) cowl and centerbody static-pressure distributions in figures 8 and 9, respectively; (3) compressor-face total-pressure profiles for various operating conditions in figures 10 to 13; (4) total bleed flows in figure 14; (5) ejector bypass operating

characteristics in figure 15; (6) performance characteristics during restarts with the corresponding diffuser static-pressure distributions and compressor-face total-pressure profiles in figures 16 to 19. Following this general presentation of the basic data, comparisons will be presented showing the effects of (a) vortex generators on total-pressure profiles during bypass operation; (b) bypass flow on peak recovery and distortion; and (c) Mach number and Reynolds number changes. In addition, the experimental and predicted restart area ratios for this inlet configuration will be compared.

Performance During Normal Operation

The performance characteristics of configurations I and IIND' without bypass flow and that of configuration IIND' with varying amounts of bypass flow are shown in figures 6 and 7, respectively, for the various Mach numbers, angles of attack, and free-stream temperature conditions. In figure 6, both configurations indicated a high performance capability at Mach 2.5. However, it was noted for configuration I that a small change in plug position caused the terminal shock to move rapidly through the throat region. With the throat bleed of configuration IIND', a small change in plug position produced a slower shock movement that was desired for a later study of shock-position dynamics. Consequently, the IIND' configuration was selected for the future phases of the overall inlet-engine investigation. Thus, the majority of the data presented are for configuration IIND' and only limited data are available for configuration I.

The mass-flow, pressure-recovery characteristics and the corresponding distortion variation without bypass flow (fig. 6) were obtained by simulating various engine speeds with the choked exit plug. With the bypass system functioning (fig. 7), the inlet characteristics were obtained both by maintaining constant bypass position and varying plug position and by maintaining constant engine corrected airflow and varying bypass flow. A comparison of figures 6 and 7 shows an increase in engine face pressure recovery when the bypass system was operating. This is primarily due to the removal of the cowl side boundary layer by the bypass. The intersections of the corrected airflow lines and the engine speed simulation curves were of particular significance for subsequent engine tests since they simultaneously matched the engine airflow demand and positioned the terminal shock such that it had a slight influence on the downstream row of centerbody bleed holes. In this manner, the shock was about the same distance downstream of the geometric throat at all Mach numbers. This terminal shock position for normal operation was based on the shock movement desired in the duct dynamics program. The simulated engine speed line was established by varying the plug position with the overboard and ejector bypass openings constant at the match point conditions. The bypass line was

determined by holding the plug position and ejector bypass settings constant and varying the overboard bypass setting.

As evident from figures 6 and 7, the inlet exhibited a moderate mass-flow range between the engine match point and inlet unstart at all Mach numbers for an angle of attack of 0°. For example, at Mach 2.5, without bypass (fig. 6) it provided about a 9-percent change in corrected airflow between the performance levels with the terminal shock in the normal operating position ($m_5/m_0 = 0.944$ and $P_5/P_0 = 0.895$) and the conditions just before inlet unstart ($m_5/m_0 = 0.889$ and $P_5/P_0 = 0.928$). With bypass flow (fig. 7) this range was increased to about 10.5 percent. This increase was a result of more flow being removed through a given bypass opening when the pressure recovery increased as the terminal shock was moved forward in the inlet. At maximum angle of attack (about 2.7°), the stable range was considerably reduced for both configurations studied.

The angle of attack at which the inlet unstarted is shown in figure 6 for different inlet operating conditions. Reducing the pressure recovery from peak inlet operation increased the unstart angle of attack, α_{un}, until a maximum value was reached. Further decrease in pressure recovery had no effect on the maximum unstart angle of attack. As Mach number was reduced from 2.6 to 2.3, both the α_{un} at peak pressure recovery and maximum α_{un} decreased. At Mach 2.6 with the centerbody translated forward to keep the tip shock ahead of the cowl lip, the contraction ratio was reduced well below the maximum allowable. Data at Mach 2.3 and control-room observations at Mach 2.0 indicated that the tolerance to angle of attack or yaw was reduced to less than 0.72°. This occurred at all operating conditions with the spike retracted to a position creating near maximum contraction ratio in the inlet at the Mach number in question. The loss was probably due to a combination of this contraction ratio and a mismatch in the cowl and centerbody contours at off-design spike positions. As a result, no data were obtained for normal operating spike positions at both Mach 2.3 and 2.0, and only the operating maps at maximum α_{un} at Mach 2.5 and 2.6 are shown in figure 7. It was also observed that translating the centerbody forward would increase tolerance to angle of attack effects but with a sacrifice in performance. This performance loss may be acceptable during short-duration maneuvers when relatively large angles of attack and/or yaw may be encountered.

Also evident, at Mach 2.5 and 2.6 (fig. 7(a) and (b)), was a discontinuity in the mass-flow, pressure-recovery characteristic near a mass-flow ratio of 0.87. This was due to a centerbody boundary-layer separation that occurred when the terminal shock was positioned on the porous surface ahead of the geometric throat. This occurrence is discussed in more detail in reference 1.

The cowl and centerbody static-pressure distributions along the top centerline over the Mach range studied and for $\alpha = 0^{\circ}$ are presented in figures 8 and 9, respectively. These distributions were obtained for the normal mode of operation; that is, operating

along the match corrected airflow line by varying the overboard bypass flow. The data obtained with and without tunnel heat were quite similar; therefore, for comparison purposes only those for elevated temperatures at Mach 2.5 are shown. The static-pressure distributions were used to provide signals for a shock-position control using the high-response bypass doors in subsequent tests.

The compressor-face total-pressure profiles shown in figures 10 to 13 correspond to the flagged points in figure 7. Only those most closely corresponding to the engine match operating conditions are shown for Mach 2.6, 2.3, and 2.0. At Mach 2.5, several operating conditions are shown. For comparable pressure recoveries resulting from either bypass or plug position variations, figures 11(c) and (f) or figures 11(d) and (g) indicate very little difference in the general shape of the profiles. Generally, the differences between hot and cold tunnel data can be attributed to the difference in Mach number due to heater operation discussed in the apparatus and procedure section. In addition, the spike position used with heater operation was optimum for the cold tunnel condition and, hence, was not necessarily optimum for the Mach number resulting from heater operation. In general, the distortion is primarily in the radial direction with only a small circumferential variation.

The total bleed flow variation with overall inlet pressure recovery is presented in figure 14 for the simulated engine speed variations shown in figure 7. Details of the flow rates in each of the bleed passages are given in reference 1. The pressure recovery of the inlet is a function of the terminal shock position which, in turn, directly affects the driving pressure on these choked bleed patterns. Consequently, the flow rates would be the same for similar shock positions regardless of whether the shock was positioned by bypass or plug position variations.

The operating characteristics of the ejector bypass used in this inlet system are shown in figure 15. These data can be used to determine the ejector flow rate at any inlet operating condition. Subtracting the sum of the ejector, bleed, and engine mass flows for any operating condition from the capture flow will give the overboard bypass flow at that condition.

Performance During Restart Cycle

Overall inlet pressure recovery and distortion during the restart cycles for the Mach range of 2.6 to 2.0 are shown in figure 16. Corresponding cowl and centerbody static-pressure distributions for the Mach 2.5 restart cycle are shown in figures 17 and 18, respectively, with the engine-face total-pressure profiles presented in figure 19. The data of figure 16 are plotted against the combined engine and overboard bypass mass flow. These data (other than started conditions at design θ_l) were obtained by varying

the bypass with the exit plug set for engine match airflow. An unstart at the design Mach number (figs. 16(b) and (c)) reduced the pressure recovery by about 50 percent and approximately doubled the distortion. In general, the unstarted inlet distortion level decreased as the centerbody was translated forward to restart. After restart, the distortion level was about the same as for the normal operating spike position. The reversal in this trend for unstarted operation at $\theta_l = 22.87^{\circ}$ is a result of a separation region in the diffuser. As shown by the total-pressure profiles of figures 19(c) and (d), these data plus other unpublished data for this inlet have shown a random circumferential location of this separation region. For the two sets of data shown, a definite separation is located in the lower left (rake 3) in figure 19(c), and a tendency for separation is indicated on top (rakes 5 to 7) in figure 19(d). When this separation region was in the top of the inlet, evidence of it can be seen from the static-pressure distributions by comparing figure 17(c) with 17(d) and figure 18(c) with 18(d). This flow separation may be associated with an unsymmetrical shock structure that was noted from schlieren observation of the conical section of the centerbody at some spike extensions with the inlet unstarted. In general, a well-defined secondary shock can also be seen in the static-pressure distributions of figures 17 and 18. These data, along with centerbody position, can provide the required signal for bypass door position control during a restart cycle. With such a control, it should be possible to minimize the distortion and maximize the pressure recovery during a restart cycle. The engine-face total-pressure profiles during the unstarted portion of the cycle (fig. 19(a) to (d)) show that the distortion is primarily circumferential. Just before restart (figs. 19(d) and (e)), and after restart (figs. 19(f) and (g)), the distortion appears to be primarily radial as previously shown in figures 10 to 13.

Effect of Vortex Generators

In other recent inlet studies (e.g., refs. 5 to 7), vortex generators have been used in short subsonic diffusers to reduce distortion levels. However, in the present inlet, their main function was to maintain attached centerbody flow at the engine face during bypass operation at moderate flow rates. In all the configurations studied (fig. 4), the generators were equally spaced around the periphery and oriented to create counter-rotating vortices. The effect of the counter rotation was to create, in the mixing zone, regions of high pressure behind the diverging (D) generator pairs. These regions, because of the mixing action, dissipate with distance. Consequently, the generators must be located far enough ahead of the compressor face for this mixing of the flow to provide the desired pressure profile free of discrete vortices. Reference 5 reports that the vortex patterns were greatly dissipated after a distance corresponding to eight pair spacings (distance between centers of D pairs). In the present investigation, the gen-

erators were spaced to make the distance from the generator station to the compressor face correspond to 4.9 and 9.8 divergent generator pair spacings for the W and N configurations, respectively. A comparison of the compressor-face total-pressure measurements at peak inlet operation behind the various vortex generator orientations with C and D generator pairs ahead of the struts is shown in figure 20. The differences in the profiles for the wide-spaced configurations (WC and WD, fig. 20(a)) indicate the presence of discrete vortices in the flow at the measuring station. This is primarily shown by rakes 7 to 9. It is also evident near the centerbody surface for rakes 5 and 6 where the low-pressure region behind a C pair of generators and the high-pressure region behind a D pair are quite obvious. The apparent lack of discrete vortices on the cowl side ahead of rakes 5 and 6 is a result of the angular location of the generators relative to the rakes (fig. 5(b)) rather than sufficient duct length for complete mixing. Due to the counter-rotating action, the centerlines of the vortices behind a D generator pair move toward each other. Consequently, they move apart behind a C pair of generators. As a result, the low-pressure region should be wider at the rake station than the high-pressure region. For configuration WD the spread of the low-pressure region behind a C pair was apparently sufficient to influence the rake measurements in the manner expected behind a C pair. Therefore, to determine whether discrete vortices are still present, the comparison should be made of measurements from a rake centered behind first one type of pair (C or D) and then the other. As shown in figure 20(b) the profiles with the close-spaced generator configurations (fig. 4(a)) installed, indicate that the flow is quite well mixed and very little evidence of discrete vortices remain. How much of the difference in the profile was due to the vortex generators or attributable to the difference in bleed configuration is not apparent. From the data presented in figure 20, it is obvious that when generators are installed, the area weighted average total-pressure recovery from stationary rakes can be greatly influenced by their location relative to the generator pairs. If sufficient mixing length is provided, the effect can be eliminated. In the present inlet system, sufficient length was provided with the narrow spacing but not with the wide spacing.

In the present configuration, a desirable compressor-face total-pressure profile was obtained with only the centerbody generators installed since the bypass uniformly removed the cowl side boundary layer. When both cowl and centerbody generators were installed, unpublished data indicated the total-pressure losses were about 2.7 percent. With just the centerbody generators about half of this loss would be eliminated. A comparison of typical total-pressure profiles with and without centerbody vortex generators is shown in figure 21 for several bypass flow rates. Without vortex generators, the profiles indicate the centerbody flow was near separation at a bypass flow rate of 12.3 percent of capture mass flow. From control-room observations, it was noted that separation occurred above 12.5 percent of capture mass flow. With vortex generator config-

uration ND' (fig. 4(a)) installed, the centerbody flow remained attached with bypass flows to about 40 percent of the maximum capture flow rate. At the same time the distortion level was reduced to approximately half the level without generators. The effect of some additional bleed is also included in these results. However, it is felt that a high percentage of the increased bypass capability and reduced distortion was due to the vortex generator action and only a small amount due to the additional bleed.

Effect of Bypass Flow

The compressor-face total-pressure recovery (with or without vortex generators) was affected when the cowl side boundary layer was removed by the bypass system. The effect of bypass flow rate on the peak performance of configuration IIND' is shown in figure 22. The inlet would not be normally operated at the peak condition because of unstart problems. However, the comparison is made at this operating point since, for the various bypass openings, the terminal shock is easily positioned in the same location relative to the bleed system. In this manner, the results shown are due to bypass alone and are not influenced by a trade-off between bleed and bypass. At all Mach numbers tested, the overall pressure recovery increased as the bypass flow was increased from 0 to about 12.5 percent of capture. For example, at Mach 2.5 the increase was from 0.92 to 0.955. Increasing the amount of bypass beyond 12.5 percent resulted in a recovery decrease. The distortion level decreased for about the same initial bypass flow range. At Mach 2.5 the decrease was from 0.08 to 0.042. The decrease at all Mach numbers was, in general, followed by an increase to about the original level or higher for bypass flow rates up to that causing centerbody flow separation (approximately 0.40 bypass mass-flow ratio). After flow separation occurs, the distortion level decreases because the separation region encompasses an increasingly larger portion of the compressor face. The one exception is at the design Mach number where the distortion level remains essentially constant from about 12.5-percent bypass up to maximum bypass; however, the characteristic shape of the curve of the other Mach numbers is apparent.

Effect of Mach Number

The effect of Mach number on the performance parameters of the inlet system is shown in figure 23. The bypass exit areas (when the bypasses were operating) were set at the match point values required at the Mach number in question except for Mach 2.0 without tunnel heat. As the Mach number was increased above design, the overall recovery decreased rapidly. Reducing the Mach number from design (2.5) to 2.3 increased

the recovery at engine match and at peak conditions by approximately 0.02 with the bypasses operating. Mach number reduction to 2.0 resulted in a 0.020 recovery loss at match conditions and 0.010 loss at peak conditions. Similar trends are shown for the configurations without bypass with the maximum recovery occurring at Mach 2.45. Generally, these data follow the theoretically predicted throat-exit pressure-recovery variation with Mach number. The scatter at the lower Mach numbers was probably a result of the differences in the overboard bypass setting at Mach 2.0 and of using the lower free-stream Mach number inlet contraction settings at Mach 2.3. The maximum available mass-flow ratio shown in figure 23 (capture minus minimum bleed flow from fig. 14) is that corresponding to the spike positions shown in figure 7. These data are for the bypass opening corresponding to the match point position for the Mach number in question. The difference between the supply and the engine demand is the required total bypass flow. As shown, the supply exceeds the demand by about 0.06 over the Mach range. The change in mass-flow ratio between engine match and peak pressure recovery was a combination of increased bleed due to terminal shock movement and more bypass due to higher overall inlet recovery. The decrease in maximum available flow at less than design Mach number was due to oblique shock spillage caused by a combination of centerbody translation and of increases in conical shock angle. Above design, the increase was due to a decrease in bleed flow caused by a combination of the movement of the internal shock structure relative to the bleeds and the reduced static pressure level in the throat bleed region. The distortion levels at match conditions (fig. 23) indicate a maximum at Mach 2.5 of about 0.11, slightly less at Mach 2.6, and decreasing to 0.08 at Mach 2.0. At peak recovery, the distortion levels indicate different trends with Mach number depending on whether the tunnel heater is used. Without tunnel heat, the distortion minimizes at about 0.04 near the design Mach number. At Mach 2.6 and 2.0, the values were 0.08 and 0.066, respectively. This trend might be anticipated since the diffuser contour in this translating centerbody inlet is on design at Mach 2.5. With tunnel heat, the distortion level is generally higher (about 0.07) and tends to be the highest around the design Mach number and lower on both ends of the Mach range studied. With the exception of the distortion levels just discussed, the variation in the other two primary inlet parameters (capture mass flow and overall recovery) was consistent with Mach number changes with or without tunnel heaters.

Effect of Reynolds Number

The results of changing Reynolds numbers from 3.82×10^6 to 1.24×10^6 (based on cowl-lip diameter) are presented in figure 24. To determine the difference in inlet performance at the different Reynolds numbers, the effect of Reynolds number on the tunnel

free-stream Mach number must be considered. For the two cases in question, the free-stream Mach number was 2.50 and 2.46 for the high and lower Reynolds number, respectively. Based on the trends with Mach number already discussed, a change in both mass-flow ratio and overall pressure recovery would be expected. The data shown in figure 23 indicate that a Mach decrease of about 0.04 should produce about a 0.018 decrease in the supercritical diffuser-exit mass-flow ratio. Based on these observations, the data of figure 24 show that a reduction in Reynolds number from 3.82×10^6 to 1.24×10^6 did not affect the inlet mass-flow ratio. Similarly, accounting for the effect of Mach number on pressure recovery from figures 23 and 6, a difference of about 0.015 at maximum recovery for maximum engine mass-flow ratio would be expected. Applying these results to the level at this condition shown in figure 24, it can be concluded that this Reynolds number reduction resulted in about a 3-percent reduction in overall total-pressure recovery. The changes in distortion level reflect the effect of Reynolds number. At the same operating condition, the distortion increased from 0.102 to 0.167 as the Reynolds number was reduced from 3.82×10^6 to 1.24×10^6. This loss of performance at the lower Reynolds number may be a result of an increased shock boundary-layer interaction at the shock impingement points because of increased boundary-layer thickness and a delay in transition. An indication of an unfavorable change in the interactions at these points was observed from unpublished centerbody and cowl static-pressure distributions. However, the exact nature of these changes could not be determined from these distributions.

Experimental and Predicted Restart Area Ratios

In a variable-geometry, mixed-compression inlet, the initial start or any restarts of supersonic flow in the inlet is usually accomplished by increasing the ratio of the throat area to the entering flow area. Mixed-compression inlets have been found to restart with less throat area than would be predicted from a one-dimensional flow analysis assuming uniform flow in front of a normal shock at the cowl lip. Experimentally determined internal area ratios required to restart the present mixed-compression inlet are presented in figure 25. As shown, this inlet also restarts at area ratios well below the normal shock values. Similar results were obtained in reference 8, which presents an analysis of restart data on a Mach 3.0 mixed-compression inlet. The reference also suggests a prediction technique based on measurements of the unstarted flow field at the point of restart. Reference 8 states that the restart flow area ratio (ratio of minimum geometric area to the measured effective flow area at the cowl lip) remained constant at a value of 0.81 for all spike extensions. This value was 0.94 of the theoretical contraction ratio for normal shock flow conditions at the cowl lip and about 1.03 times the theoretical contraction ratio for the miltiple-shock flow field resulting from the oblique

shock induced by the centerbody boundary-layer separation. To estimate restart area ratios for the present inlet over the Mach number range, it was assumed that the restart flow areas maintained the same relation to the theoretical multiple shock and normal shock contraction ratios of 1.03 and 0.94, respectively. Reference 9 was used to predict the separation wedge angle required to determine the local flow conditions in the multishock region. As shown in figure 25, the predicted values are 2 percent low at the design Mach number of 2.5, 1.3 percent low at Mach 2.3, and identical to measured values at Mach 2.0. The results indicate that this technique, as suggested by reference 8 along with the assumptions used in the present analysis, accurately predicted the required restart area ratios for the present inlet over the test Mach number range. The experimental results also compare quite favorably with a no-bleed, all-internal-compression inlet designed for Mach 3.0. The area ratios shown for that inlet were obtained from reference 8. With the spike translated forward to the restart position, the present Mach-2.5 inlet can also be considered a no-bleed configuration because the cowl bleeds are well downstream of the throat and the forward centerbody bleed removes enough flow so that the actual restart minimum area, A_{min}, occurs at the leading edge of the forward centerbody bleed.

SUMMARY OF RESULTS

A cold-pipe investigation was conducted to determine the performance characteristics of an axisymmetric, mixed-compression inlet system designed for Mach 2.5 and to match the J-85/13 turbojet engine. Sixty percent of the overall supersonic area contraction occurred internally. The spike could be translated to vary internal contraction ratio. The inlet also included two operating bypass systems: a high-response overboard system for shock-position control and a low-speed valve to control secondary flow through the nacelle for engine and ejector cooling.

Data were obtained over the Mach range of 1.98 to 2.58. The Reynolds number varied from 1.24×10^6 to 3.82×10^6 based on inlet cowl-lip diameter. Both zero angle of attack and the maximum angle before an inlet unstart occurred were studied. The following results were obtained:

1. At zero angle of attack, a moderate stable operating range between match conditions and inlet unstart was obtained at all Mach numbers without large sacrifices in performance. At Mach 2.5, this range amounted to about 10.5 percent of design engine corrected airflow. At maximum unstart angle of attack of about 2.7°, this range was sizeably reduced.

2. Flow bypass of up to 12.5 percent of capture mass flow increased the inlet pressure recovery and reduced the distortion at all Mach numbers studied.

3. Use of vortex generators on the centerbody prevented flow separation from the centerbody for bypass flows up to about 40 percent of capture.

4. As the Mach number was decreased from 2.5 to 2.3 (with bypasses open to match point exit areas) the match pressure recovery increased by about 1.6 percent. Reducing the Mach number from 2.3 to 2.0 resulted in a 2.2 percent reduction in the match-condition pressure recovery. Above Mach 2.5 the pressure recovery decreased rapidly.

5. At engine match conditions, the distortion was a maximum of 0.11 at Mach 2.5, slightly less at Mach 2.6, and decreased to 0.08 at Mach 2.0.

6. The effect of reducing the Reynolds number from 3.82×10^6 to 1.24×10^6 at Mach 2.5 was to reduce the overall pressure recovery by approximately 3 percent at maximum recovery for maximum engine mass-flow ratio. The corresponding distortion levels increased from 0.102 to 0.167. No change in diffuser exit mass-flow ratio was indicated.

7. The inlet restarted at all test Mach numbers with throat areas smaller than required to pass the flow through a simple normal shock. A technique suggested in reference 8 predicted restart area ratios that were within 98 percent of the experimentally determined values.

Lewis Research Center,
National Aeronautics and Space Administration,
Cleveland, Ohio, October 2, 1968,
126-15-02-11-22.

REFERENCES

1. Cubbison, Robert W.; Meleason, Edward T.; and Johnson, David F.: Effect of Porous Bleed in a High-Performance Axisymmetric, Mixed-Compression Inlet at Mach 2.50. NASA TM X-1692, 1968.

2. Sanders, Bobby W.; and Cubbison, Robert W.: Effect of Bleed-System Back Pressure and Porous Area on the Performance of an Axisymmetric, Mixed-Compression Inlet at Mach 2.50. NASA TM X-1710, 1968.

3. Sorensen, Virginia L.: Computer Program for Calculating Flow Fields in Supersonic Inlets. NASA TN D-2897, 1965.

4. Cubbison, Robert W.; and Meleason, Edward T.: Water Condensation Effects of Heated Vitiated Air on Flow in a Large Supersonic Wind Tunnel. NASA TM X-1636, 1968.

5. Mitchell, Glenn A.; and Davis, Ronald W.: Performance of Centerbody Vortex Generators in an Axisymmetric Mixed-Compression Inlet at Mach Numbers From 2.0 to 3.0. NASA TN D-4675, 1968.

6. Sorensen, Norman E.; and Smeltzer, Donald B.: Investigation of a Large-Scale Mixed Compression Axisymmetric Inlet System Capable of High Performance at Mach Numbers 0.6 to 3.0. NASA TM X-1507, 1968.

7. Sorensen, Norman E.; Cubbison, Robert W.; and Smeltzer, Donald B.: Study of a Family of Supersonic Inlet Systems. Paper No. 68-580, AIAA, June 1968.

8. Mitchell, Glenn A.; and Cubbison, Robert W.: An Experimental Investigation of the Restart Area Ratio of a Mach 3.0 Axisymmetric Mixed Compression Inlet. NASA TM X-1547, 1968.

9. Nussdorfer, T. J.: Some Observations of Shock-Induced Turbulent Separation on Supersonic Diffusers. NACA RM E51L26, 1954.

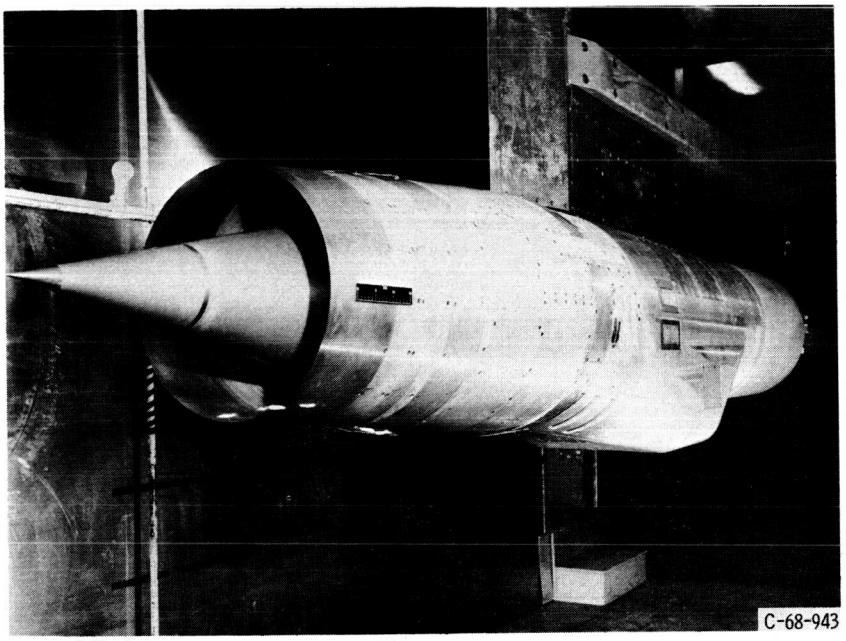

Figure 1. - Model installed in 10- by 10-foot Supersonic Wind Tunnel test section.

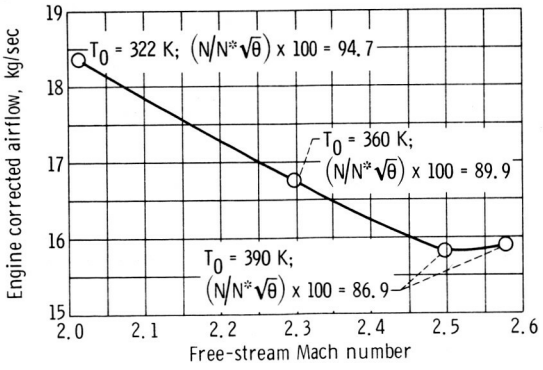

Figure 2. - Assumed engine airflow schedule selected for inlet-engine interaction studies.

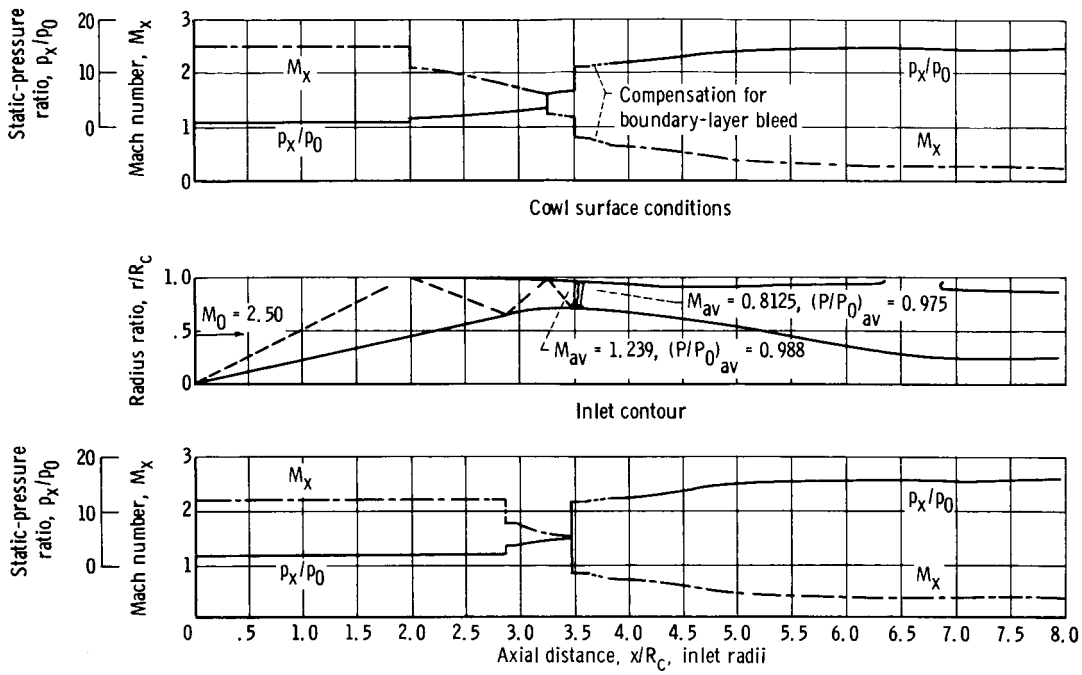

(a) Inlet dimensions and theoretical flow conditions.

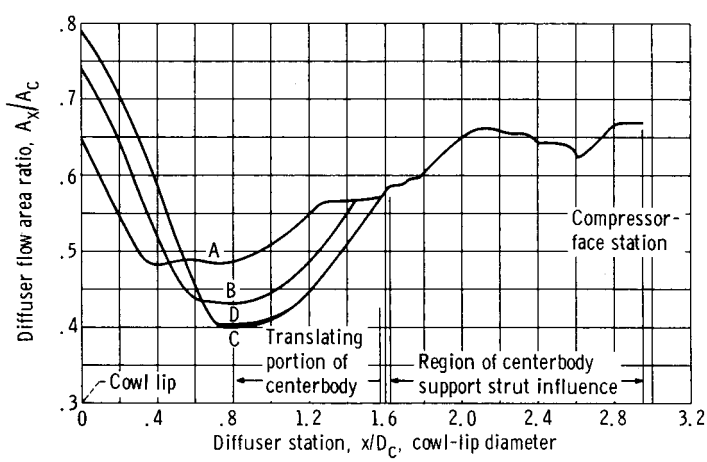

	Free-stream Mach number, M_0	Cowl-lip position parameter, θ_l, deg
A	2.02	20.6
B	2.20	23.87
C	2.50	26.6
D	2.58	26.23

(b) Diffuser area variation.

Figure 3. - Aerodynamic details.

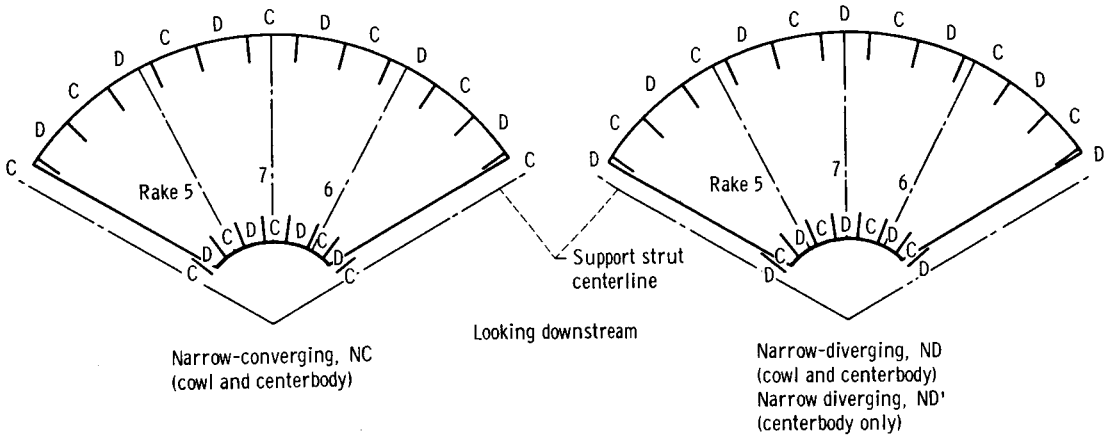

Configurations

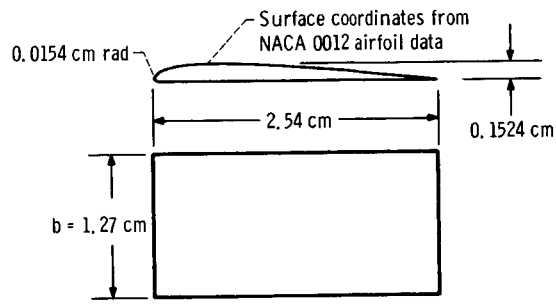

Generator details

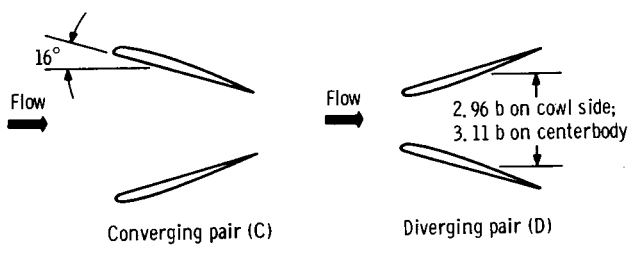

Generator orientation

(a) Narrow spaced vortex generators for modified NACA 0012 airfoil.

Figure 4. - Vortex generator design.

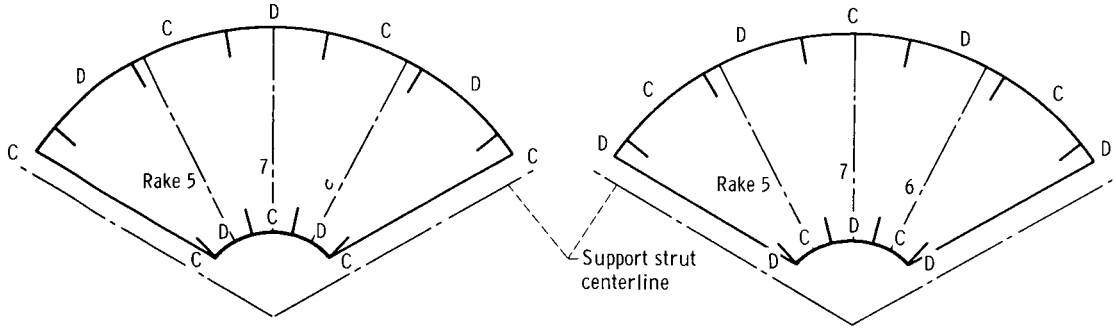

Looking downstream

Wide-converging

Wide-diverging

Configurations

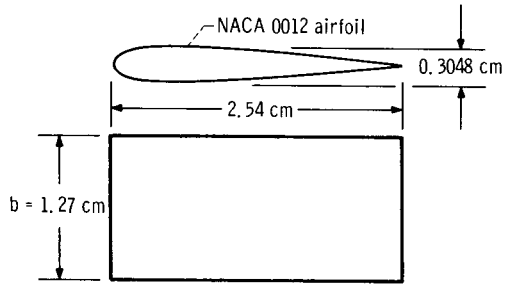

Generator details

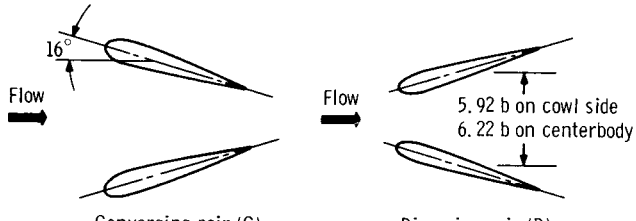

Converging pair (C)

Diverging pair (D)

Generator orientation

(b) Wide spaced vortex generators for NACA 0012 airfoil.

Figure 4. - Concluded.

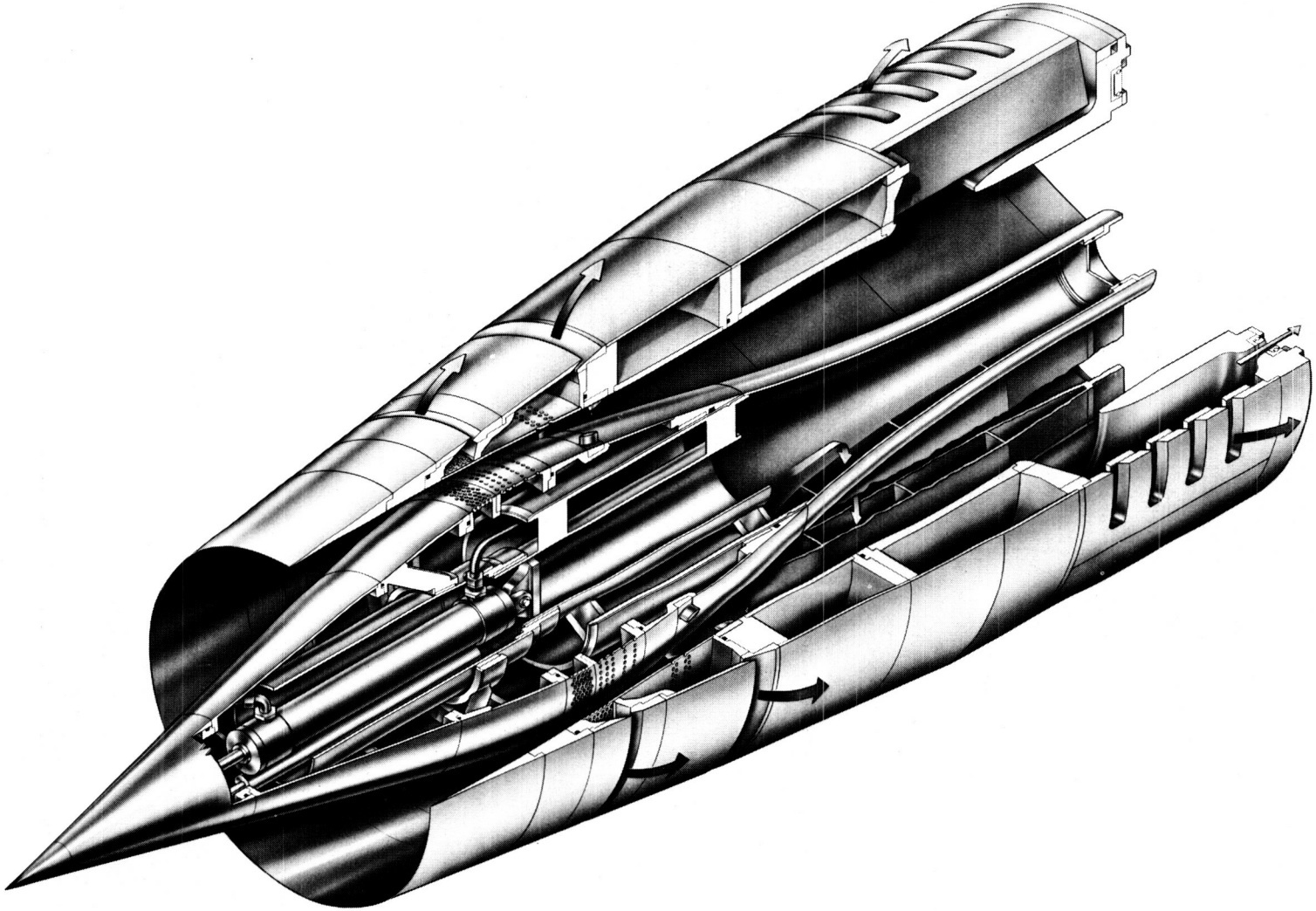

(a) Isometric view of model.

Figure 5. - Model details.

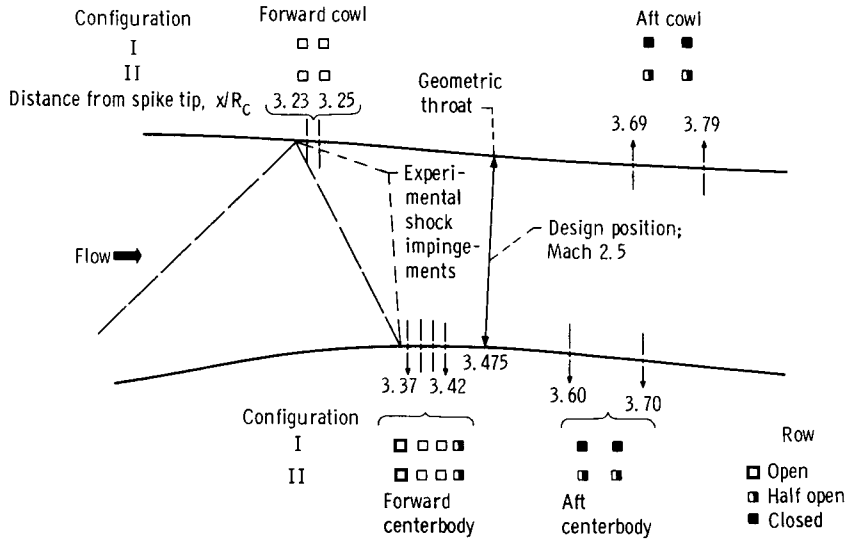

(b) Bleed configuration. Bleed hole diameter, 0.3175 centimeter.

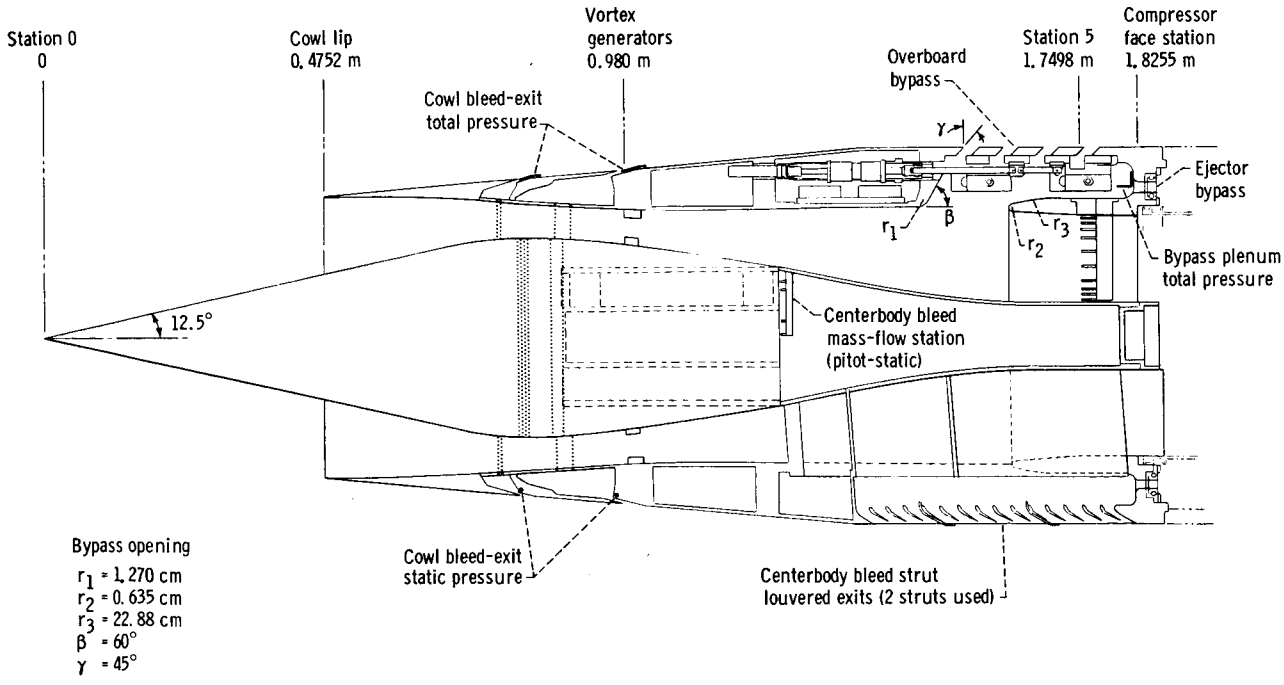

CD-9063

(c) Pressure instrumentation and bypass entrance dimensions (all stations referenced to M_0 = 2.498 centerbody location.).

Figure 5. - Continued.

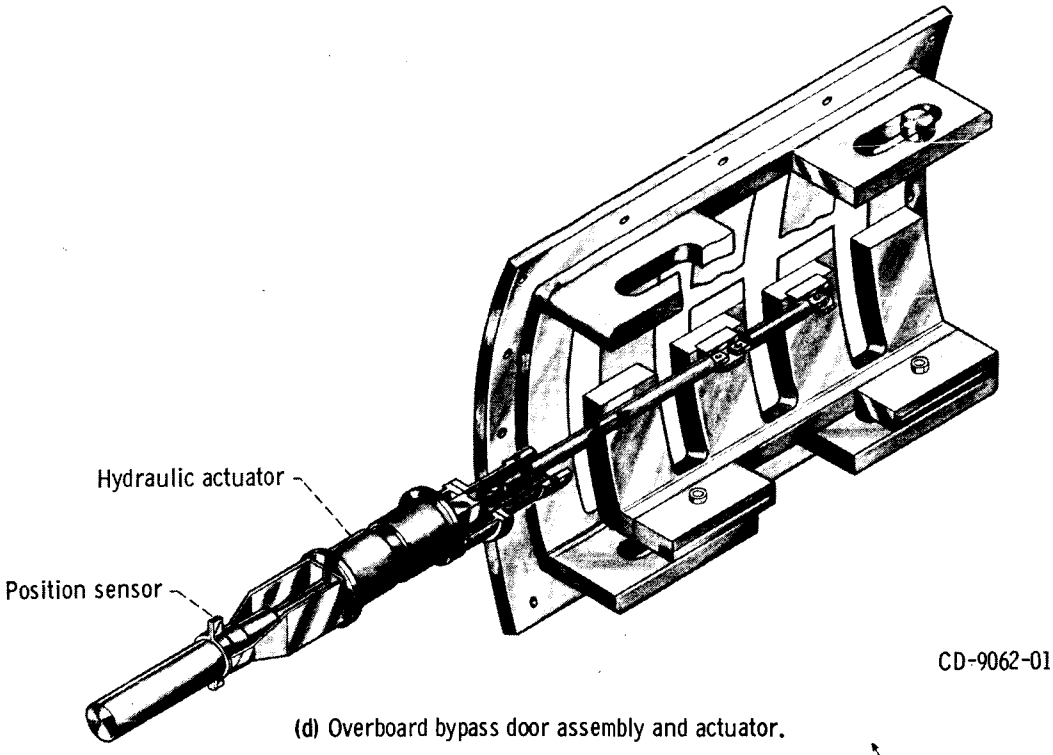

(d) Overboard bypass door assembly and actuator.

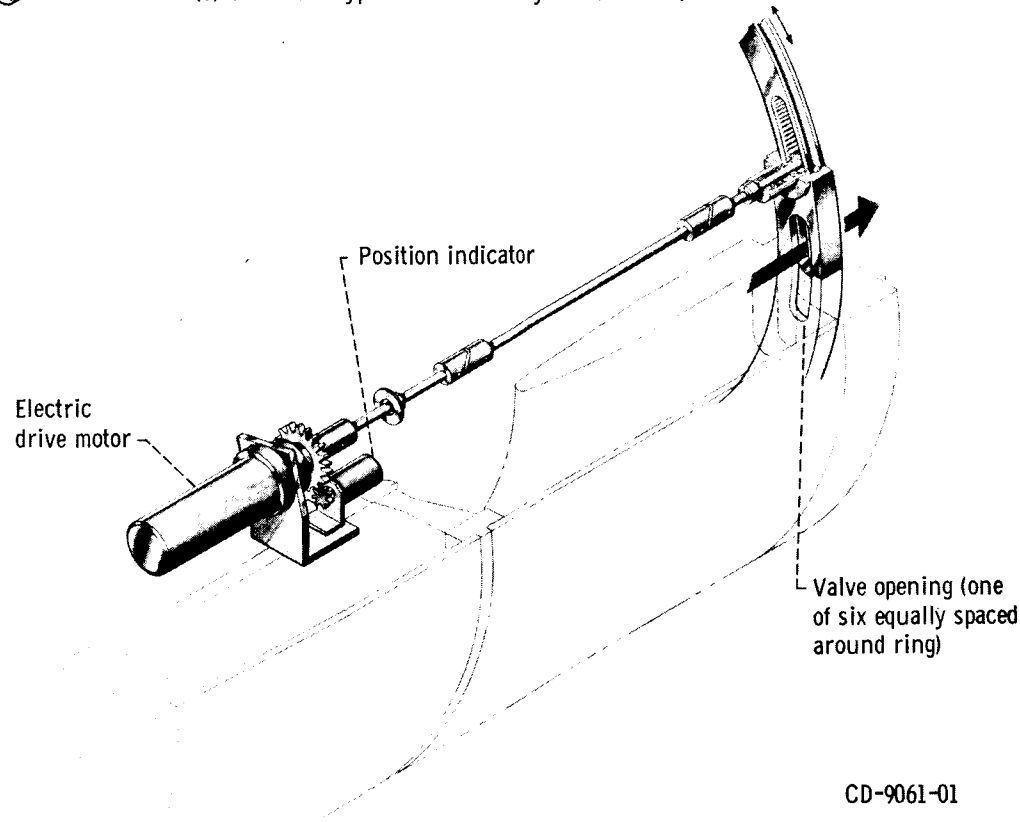

(e) Ejector bypass valve and actuator.

Figure 5. - Continued.

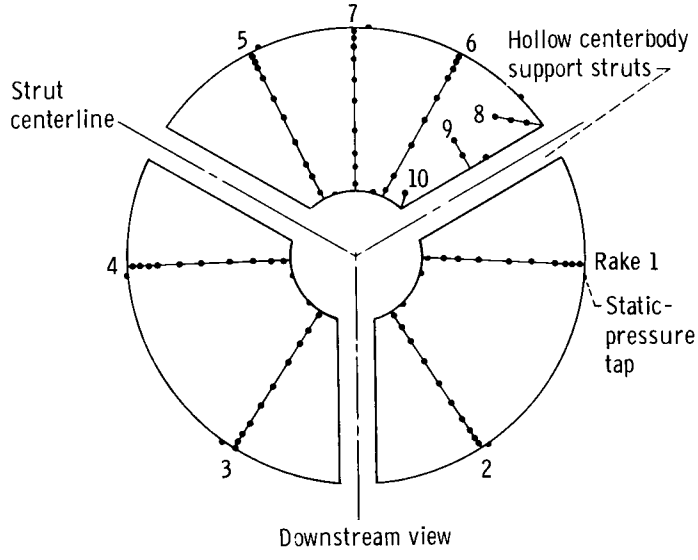

(f) Total- and static-pressure instrumentation at diffuser station 5.

Figure 5. - Concluded.

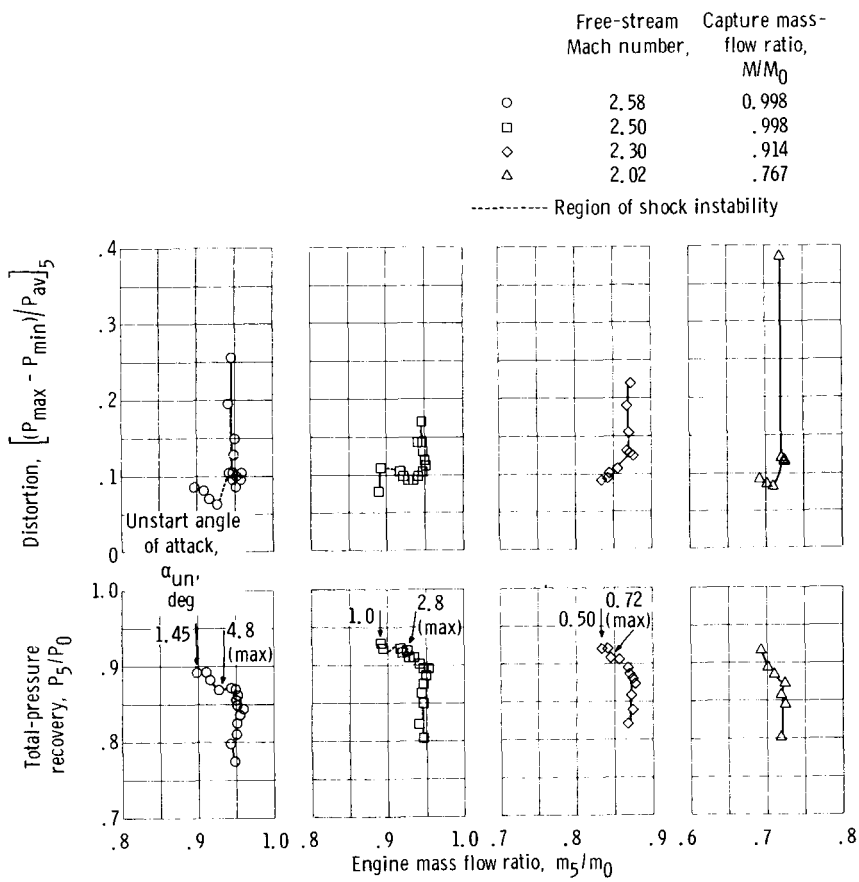

(a-1) Free-stream temperature, 373 K; cowl-lip-position parameter, 26.23°; Reynolds number, 3.45×10^6.

(a-2) Free-stream temperature, 317 K; cowl-lip-position parameter, 26.6°; Reynolds number, 3.82×10^6.

(a-3) Free-stream temperature, 317 K; cowl-lip-position parameter, 23.87°; Reynolds number, 3.82×10^6.

(a-4) Free-stream temperature, 317 K; cowl-lip-position parameter, 20.6°; Reynolds number, 3.82×10^6.

(a) Configuration IIND'; angle of attack, 0.

Figure 6. - Overall inlet performance without bypass flow.

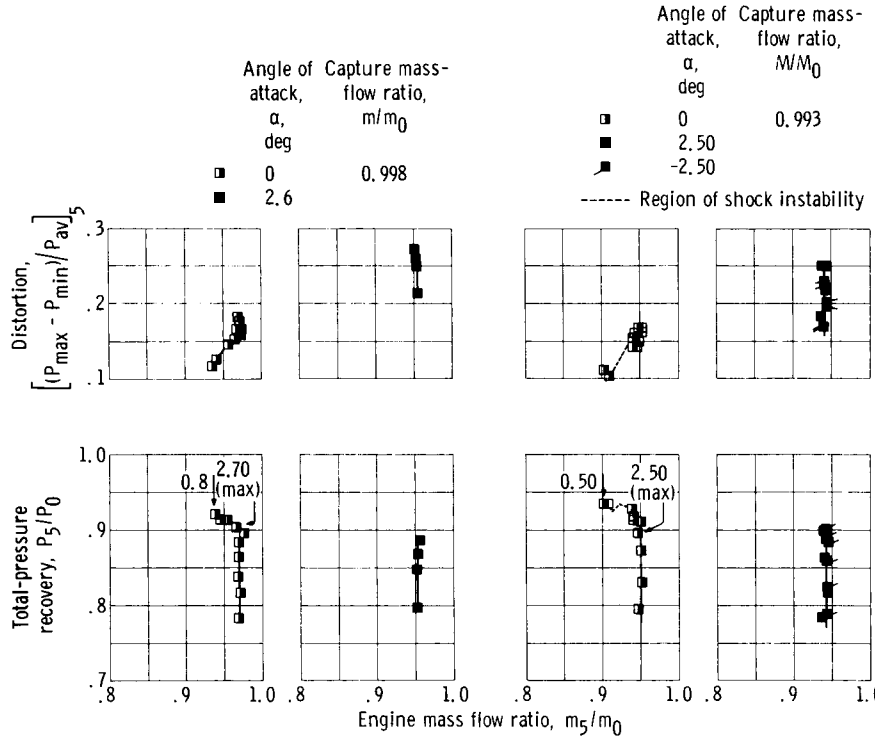

(b) Configuration I; free-stream temperature, 317 K; free-stream Mach number, 2.50; Reynolds number, 3.82×10^6; cowl-lip-position parameter, 26.6°.

(c) Configuration I; free-stream temperature, 400 K; free-stream Mach number, 2.46; Reynolds number, 3.24×10^6; cowl-lip-position parameter, 26.6.

Figure 6. - Concluded.

	Capture mass-flow ratio, $(m/m_0)_{capt}$	Reynolds number, Re	Free-stream Mach number, M_0	Angle of attack, α, deg	Free-stream temperature, T_0, K
○	0.998	3.45×10^6	2.58	0	373
□		3.45	2.58	4.80	373
△	.993	3.24	2.55	0	391
◇		3.24	2.55	4.80	391

--------- Region of shock instability

Tailed symbols denote total-pressure profiles (see fig. 10)
Open symbols denote engine airflow variation using choked exit plug
Solid symbols denote performance at constant engine corrected airflow by varying overboard bypass exit area

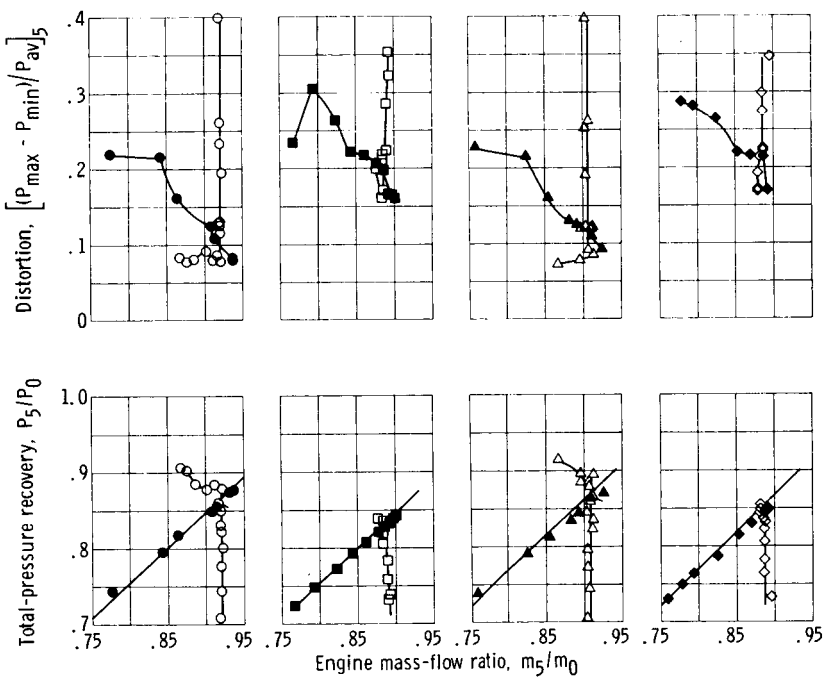

(a) Nominal free-stream Mach number, 2.6; cowl-lip-position parameter, 26.23°; ejector area to capture area ratio, 0.0075; engine corrected airflow, 15.89 kilograms per second.

Figure 7. - Overall performance of inlet configuration IIND with bypass flow.

	Capture mass-flow ratio, $(m/m_0)_{capt}$	Reynolds number, Re	Free-stream Mach number, M_0	Angle of attack, α, deg	Free-stream temperature, T_0, K
○	0.998	3.82×10^6	2.50	0	317
□		3.82	2.50	2.7	317
△	.993	3.24	2.47	0	390
◇		3.24	2.47	2.5	390

------- Region of shock instability

Tailed symbols denote total-pressure profiles (see fig. 11)
Open symbols denote engine airflow variation using choked exit plug
Solid symbols denote performance at constant engine corrected airflow by varying overboard bypass exit area

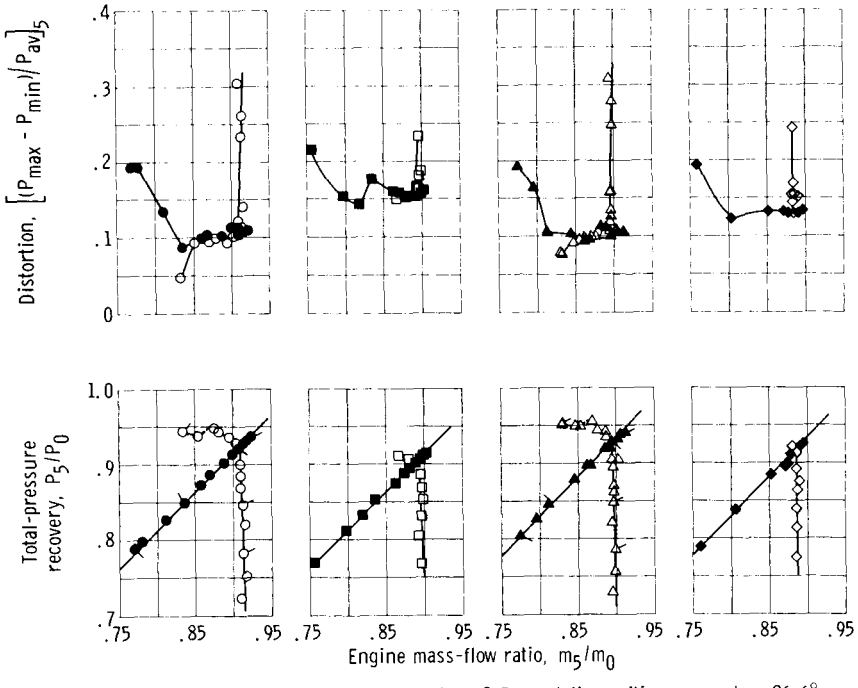

(b) Nominal free-stream Mach number, 2.5; cowl-lip-position parameter, 26.6°; ejector area to capture area ratio, 0.0081; engine corrected airflow, 15.83 kilograms per second.

Figure 7. - Continued.

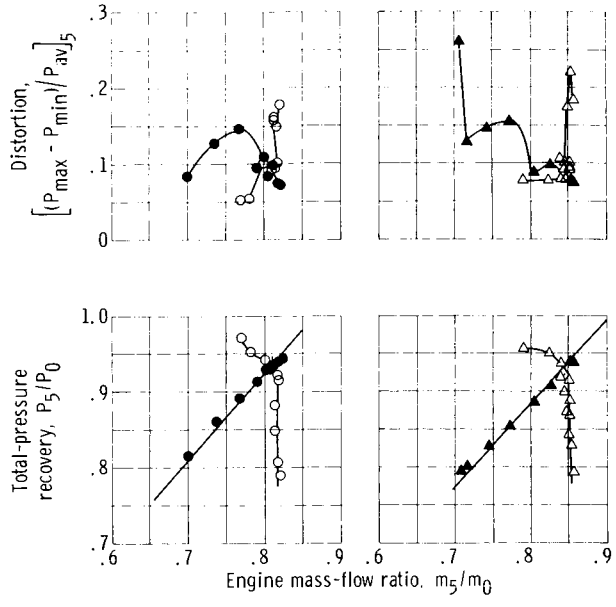

	Capture mass-flow ratio, $(m/m_0)_{capt}$	Reynolds number, Re	Free-stream Mach number, M_0	Free-stream temperature, T_0, K
○	0.914	3.82×10^6	2.30	317
△	.921	3.37	2.34	362

Tailed symbols denote total-pressure profiles (see fig. 12)
Open symbols denote engine airflow variation using choked exit plug
Solid symbols denote performance at constant engine corrected airflow by varying bypass exit area

(c) Nominal free-stream Mach number, 2.3; cowl-lip-position parameter, 23.87°; angle of attack, 0°; ejector area to capture area ratio, 0.0076; engine corrected airflow, 16.75 kilograms per second.

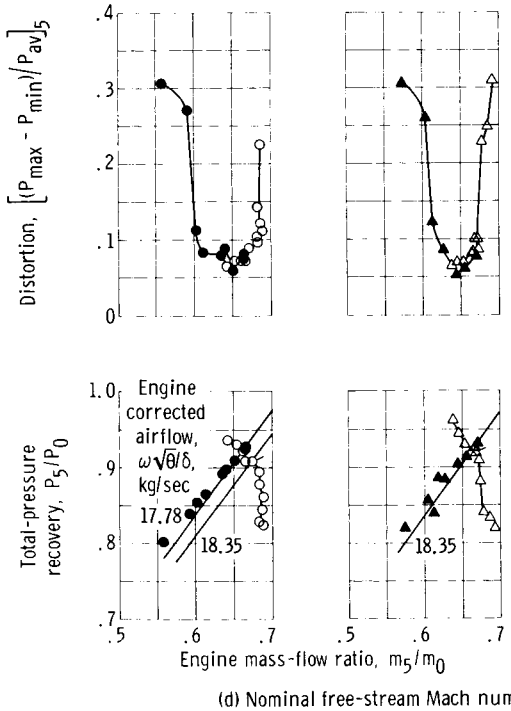

	Capture mass-flow ratio, $(m/m_0)_{capt}$	Reynolds number, Re	Free-stream Mach number, M_0	Free-stream temperature, T_0, K	Ejector area to capture area ratio, A_{ej}/A_c
○	0.767	3.82×10^6	2.02	317	0.0236
△	.762	3.48	1.98	324	.0248

Tailed symbols denote total-pressure profiles (see fig. 13)
Open symbols denote engine airflow variation using choked exit plug
Solid symbols denote constant engine corrected airflow by varying overboard bypass exit area

(d) Nominal free-stream Mach number, 2.0; cowl-lip-position parameter, 20.6°; angle of attack, 0°.

Figure 7. - Concluded.

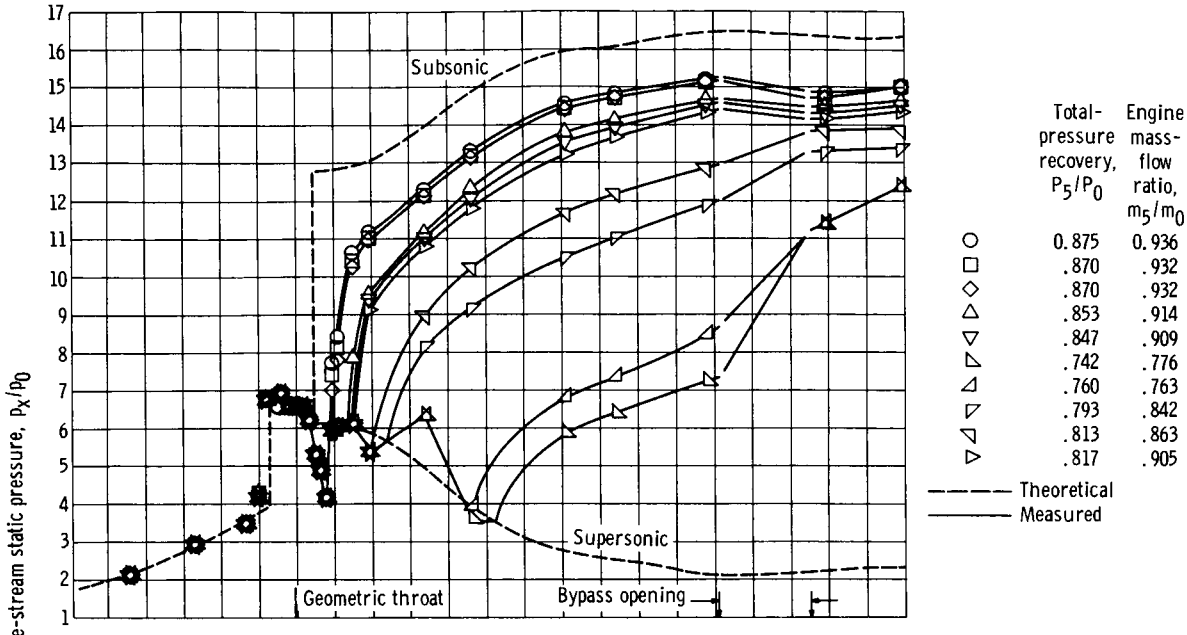

(a) Free-stream Mach number, 2.58; free-stream temperature, 373 K; cowl-lip-position parameter, 26.23°.

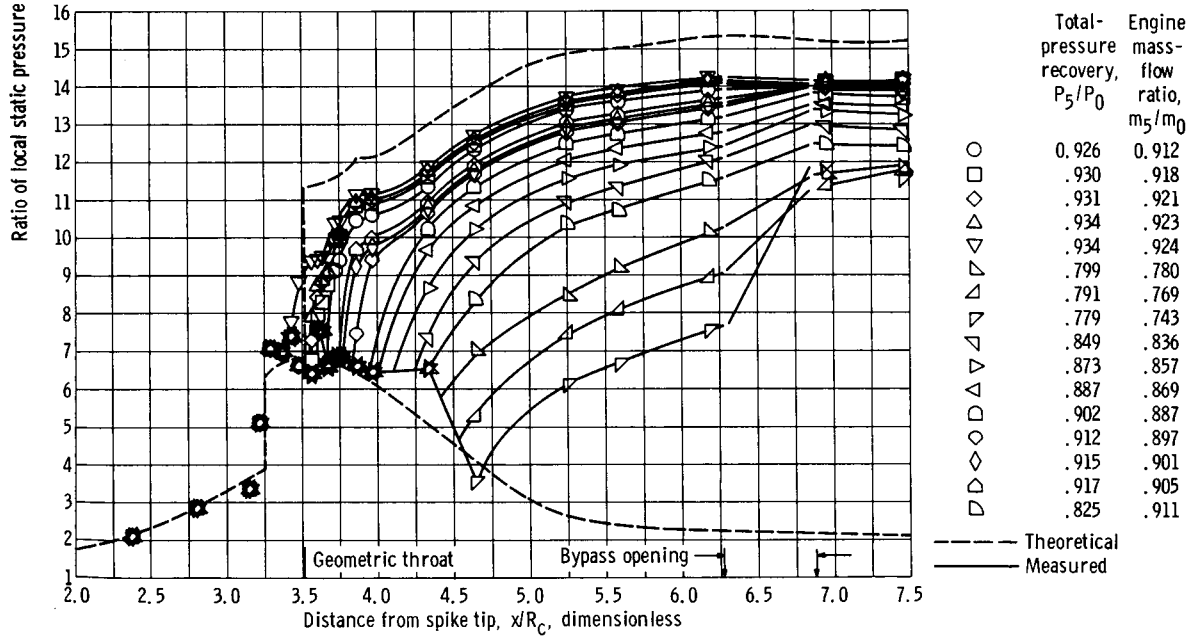

(b) Free-stream Mach number, 2.50; free-stream temperature, 317 K; cowl-lip-position parameter, 26.6°.

Figure 8. - Internal cowl surface static-pressure distributions for various bypass door settings and engine match corrected airflow. Configuration IIND'; angle of attack, 0°.

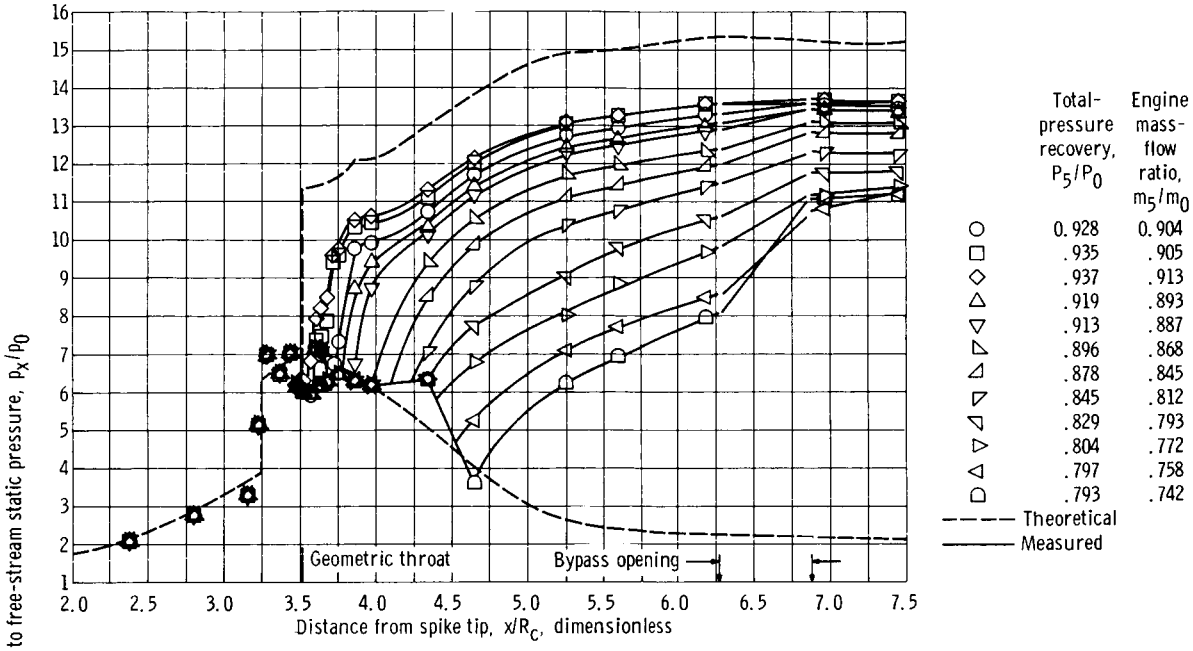

(c) Free-stream Mach number, 2.47; free-stream temperature 390 K; cowl-lip-position parameter, 26.6°.

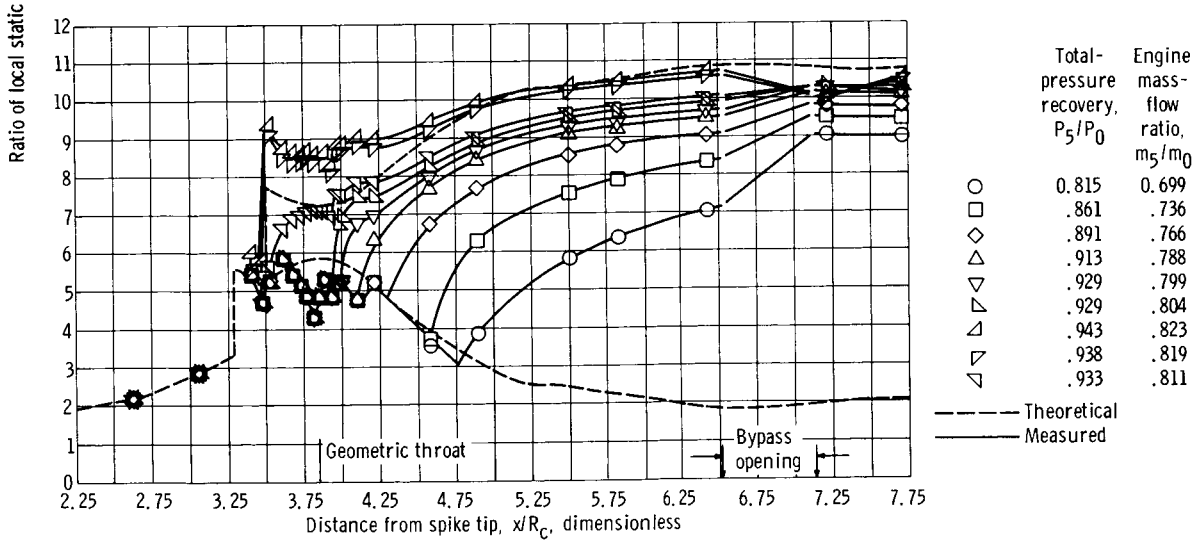

(d) Free-stream Mach number, 2.30; free-stream temperature, 317 K; cowl-tip-position parameter, 23.87°.

Figure 8. - Continued.

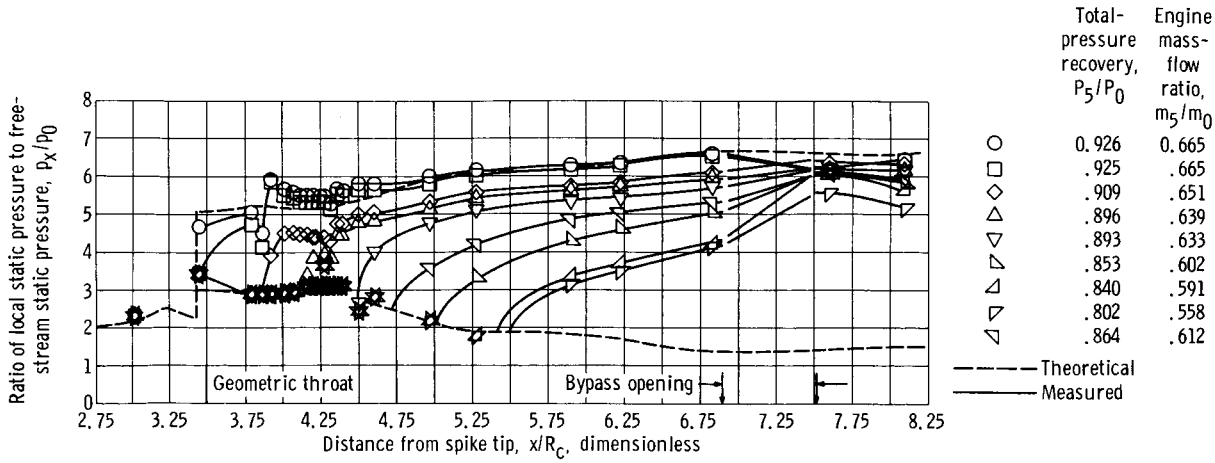

(e) Free-stream Mach number, 2.02; free-stream temperature, 317 K; cowl-lip-position parameter, 20.6°.

Figure 8. - Concluded.

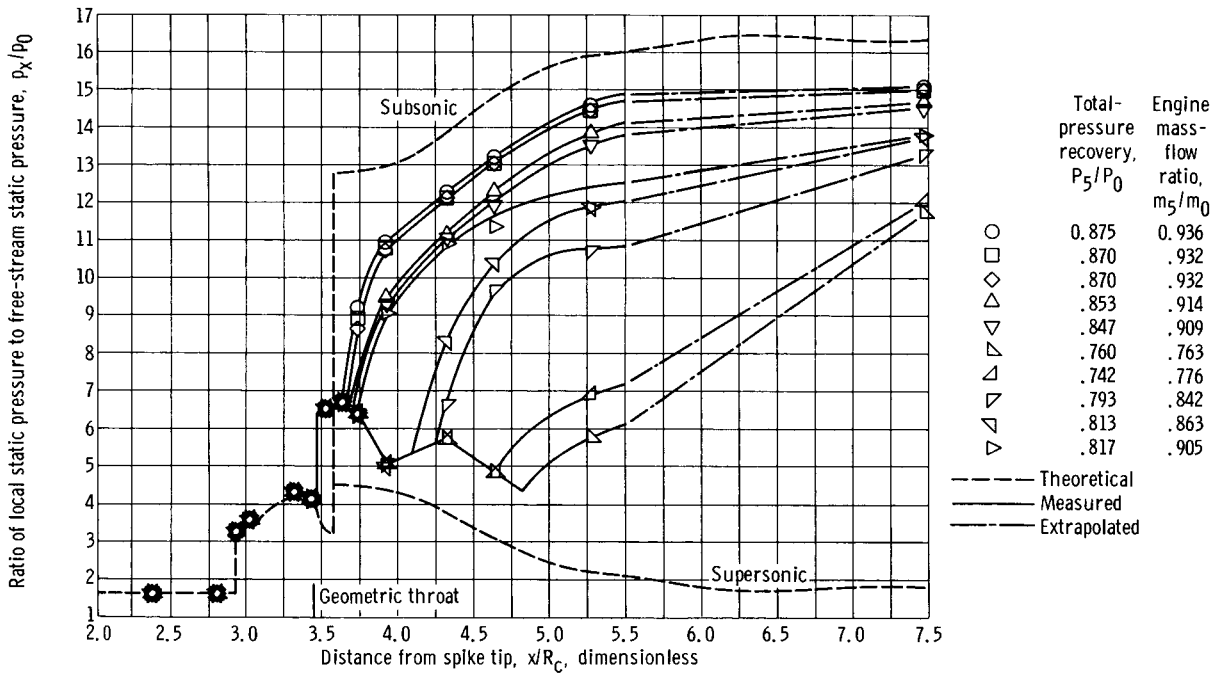

(a) Free-stream Mach number, 2.58; free-stream temperature, 373 K; cowl-lip-position parameter, 26.23°.

Figure 9. - Centerbody surface static pressure distributions for various bypass door settings and engine match corrected airflow. Configuration IIND'; angle of attack, 0°.

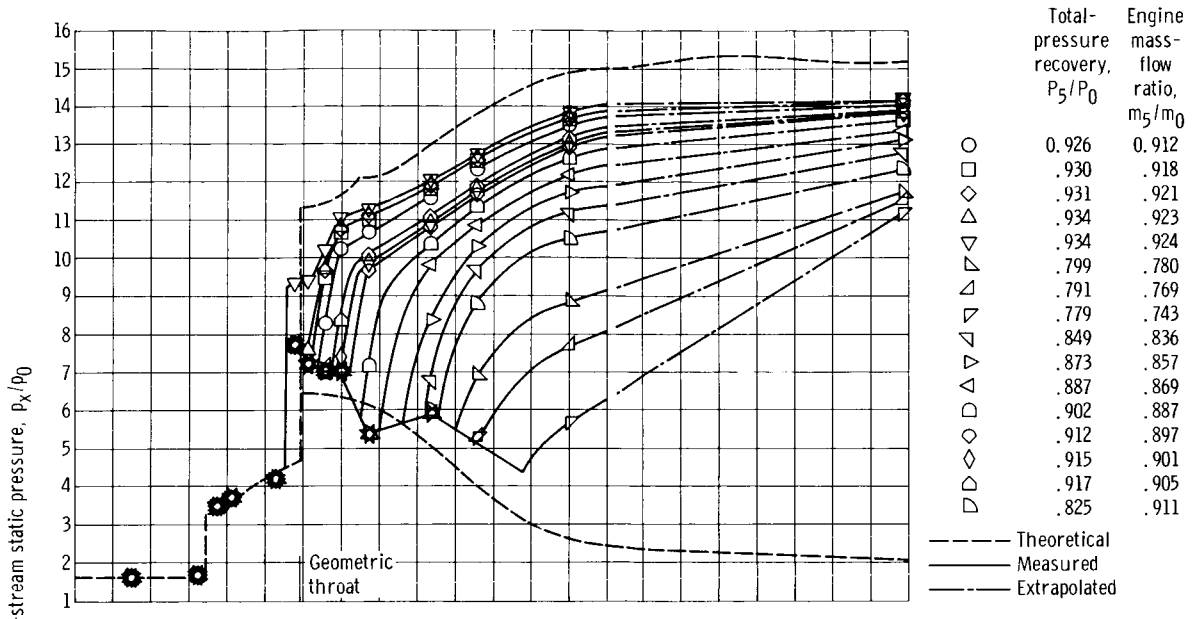

(b) Free-stream Mach number, 2.50; free-stream temperature, 317 K; cowl-lip-position parameter, 26.6°.

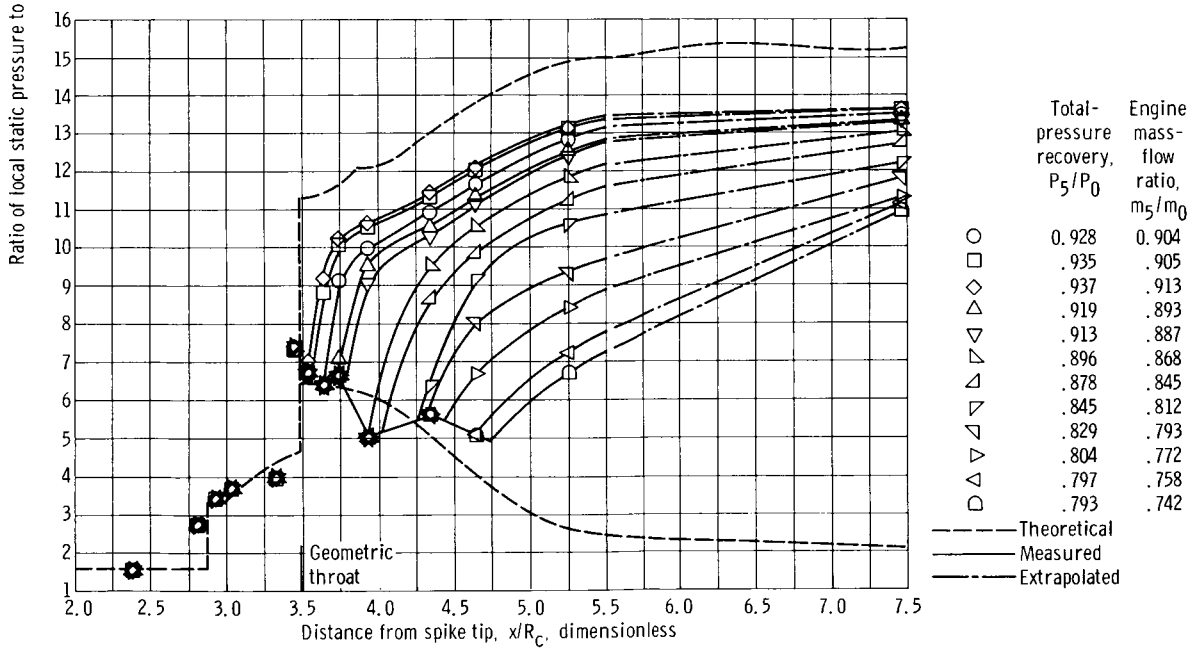

(c) Free-stream Mach number, 2.47; free-stream temperature, 390 K; cowl-lip-position parameter, 26.6°.

Figure 9. - Continued.

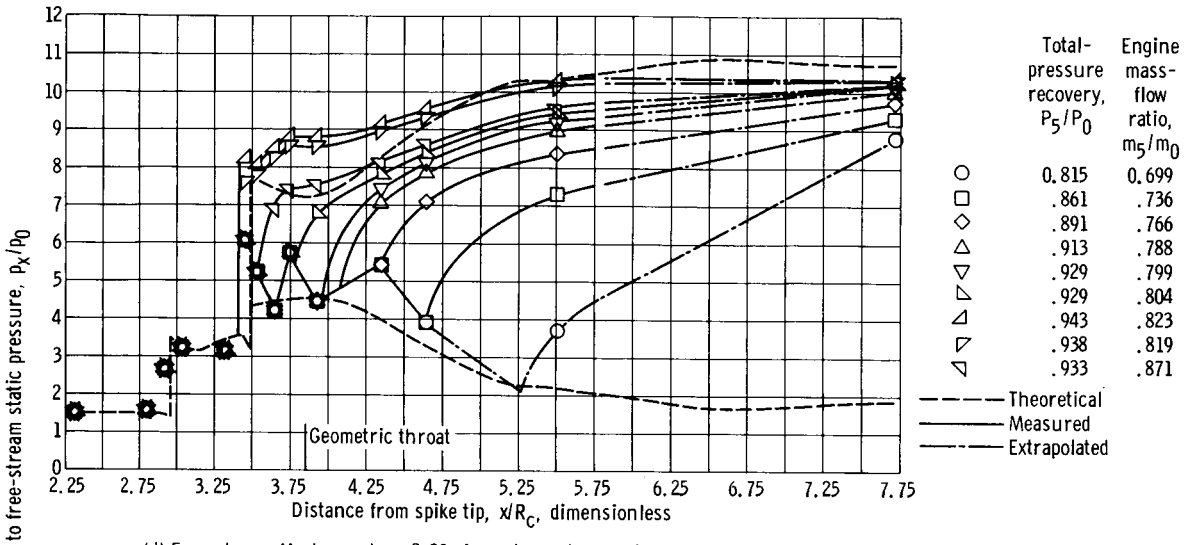

(d) Free-stream Mach number, 2.30; free-stream temperature, 317 K; cowl-lip-position parameter, 23.87°.

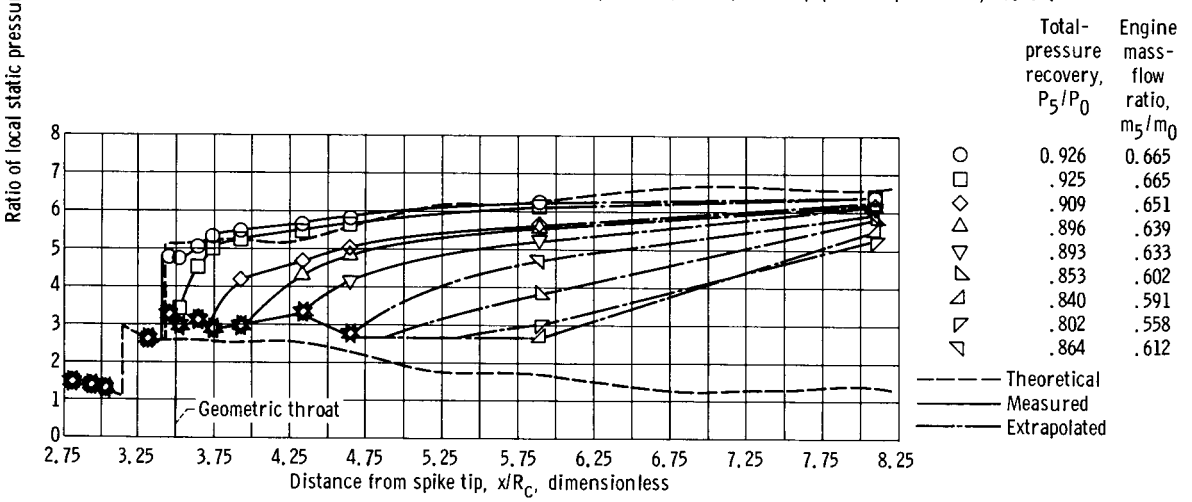

(e) Free-stream Mach number, 2.02; free-stream temperature, 317 K; cowl-lip-position parameter, 20.6°.

Figure 9. - Concluded.

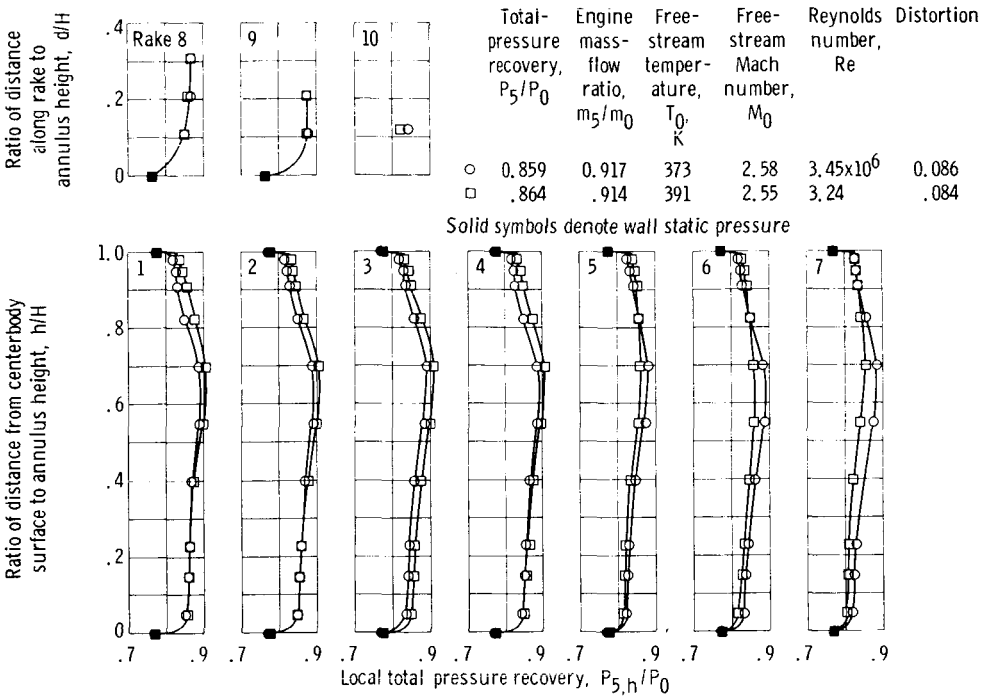

Figure 10. - Comparison of compressor-face total-pressure profiles at engine match conditions with and without tunnel heat. Configuration IIND'; nominal free-stream Mach number, 2.6; angle of attack, 0°; ejector area to capture area ratio, 0.0075.

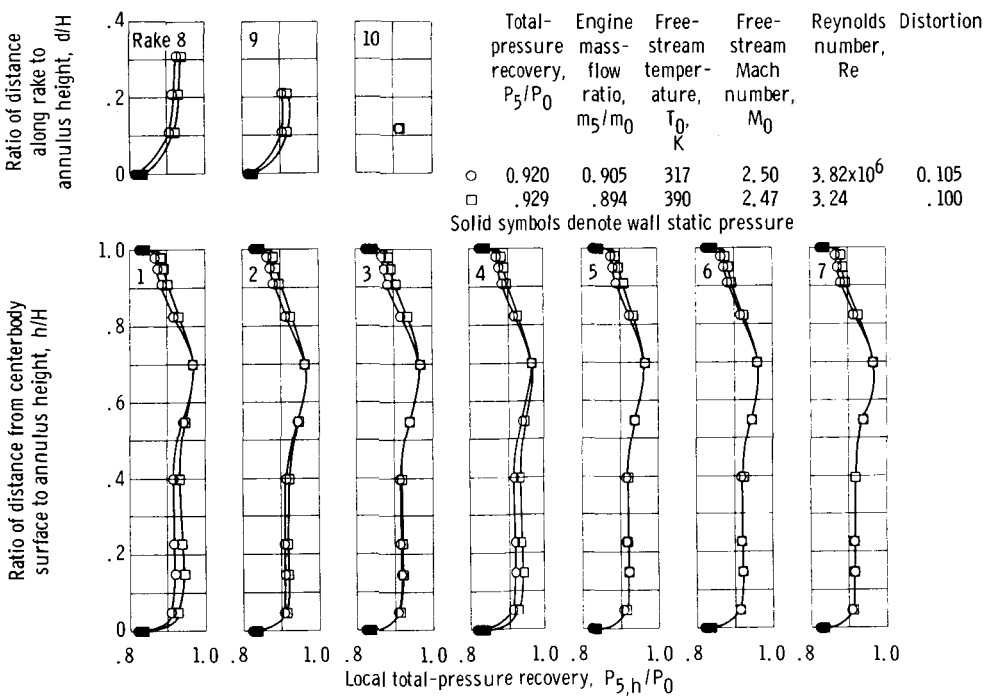

(a) Engine match corrected airflow; bypass set at match opening.

Figure 11. - Comparison of compressor-face total-pressure profiles at various operating conditions with and without tunnel heat. Configuration IIND'; nominal free-stream Mach number, 2.5; angle of attack, 0°; ejector area to capture area ratio, 0.0081.

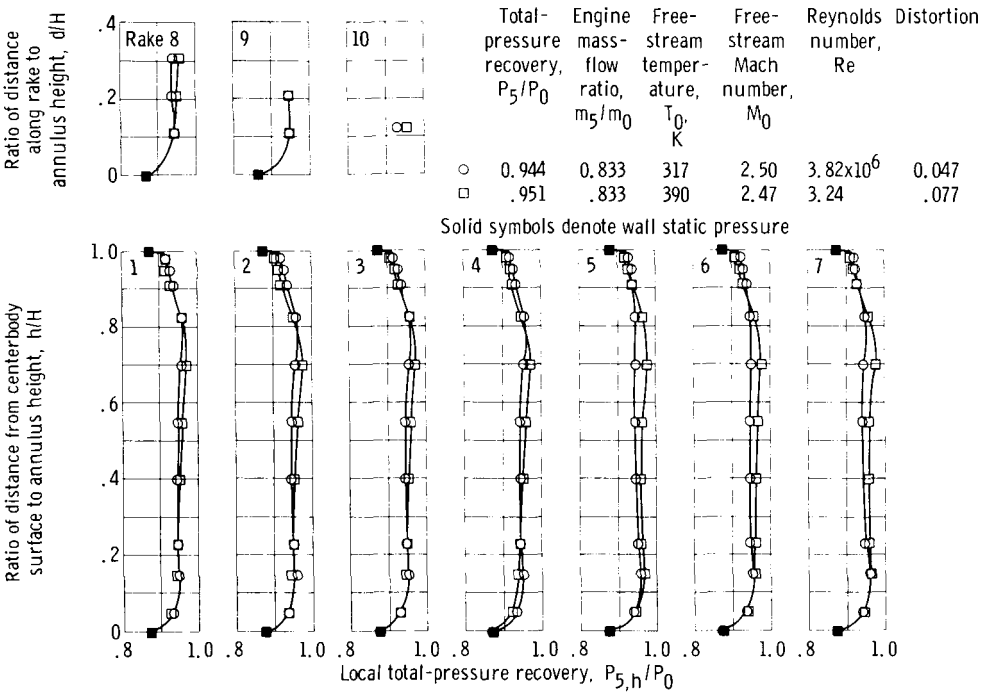

(b) 90 Percent of engine match corrected airflow; bypass set at match opening.

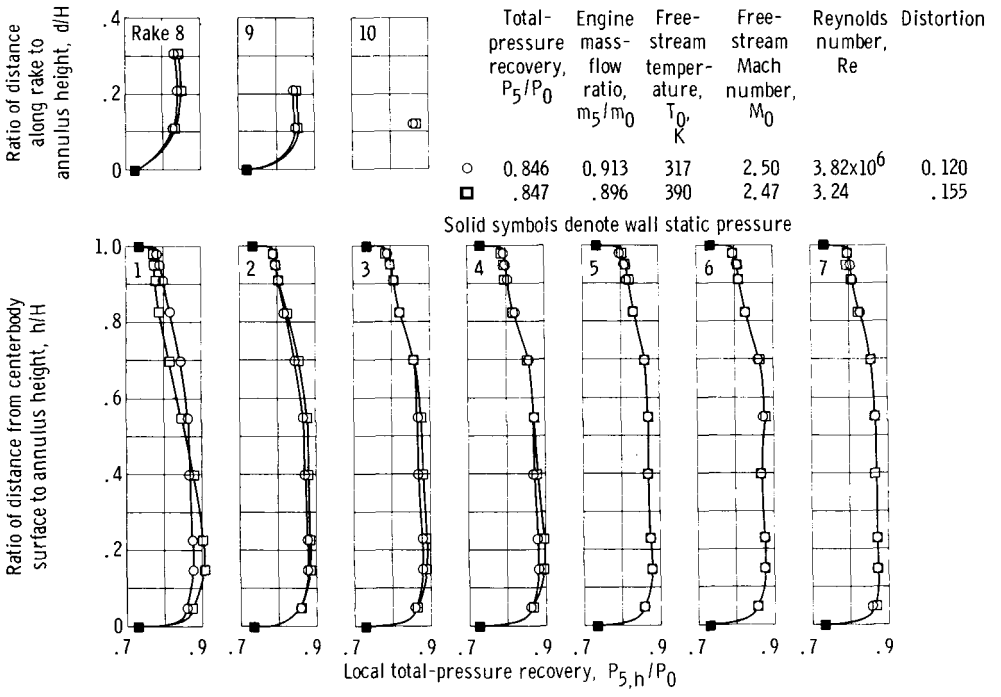

(c) 110 Percent of engine match corrected airflow; bypass set at match opening.

Figure 11. - Continued.

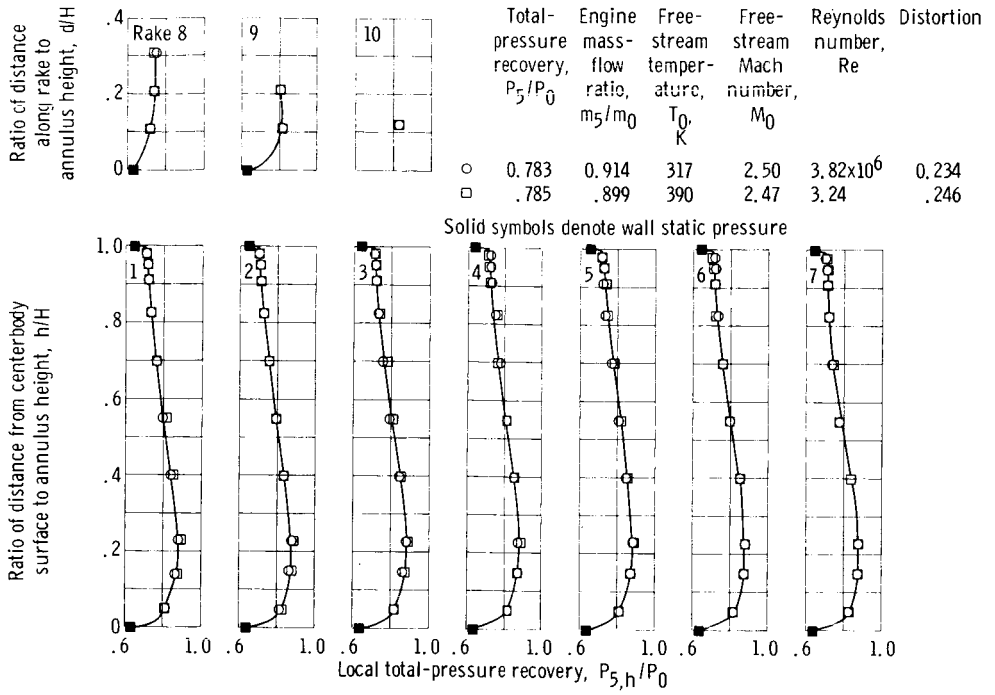

(d) 119 Percent of engine match corrected airflow; bypass set at match opening.

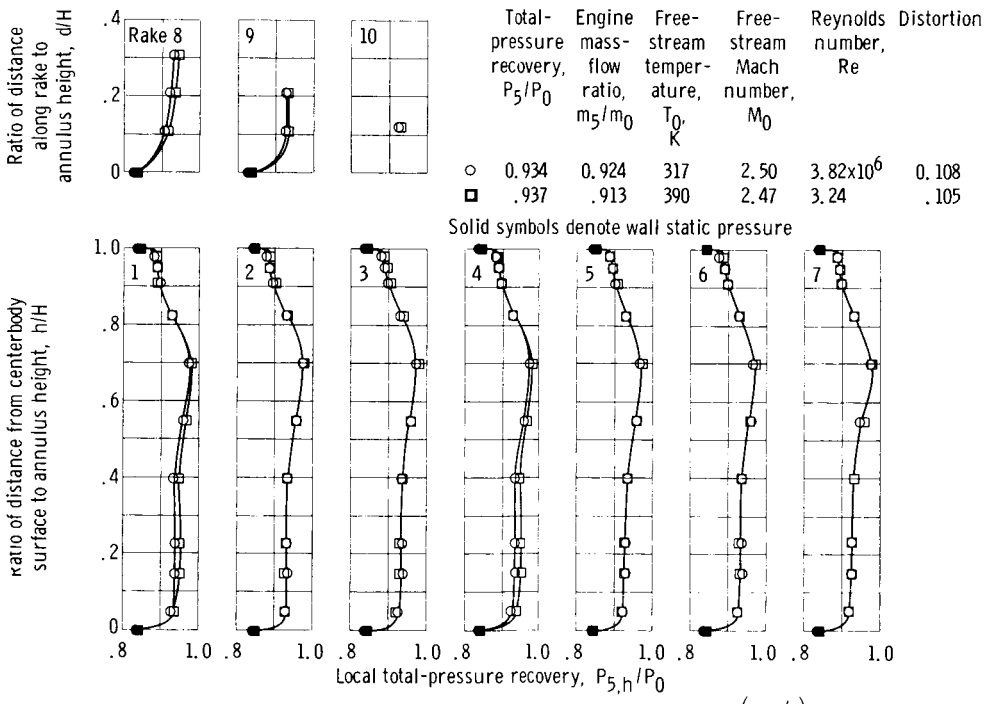

(e) 101.5 Percent of match pressure recovery set with bypass; $\left(w\sqrt{\theta}/\delta\right)_5$ = match.

Figure 11. - Continued.

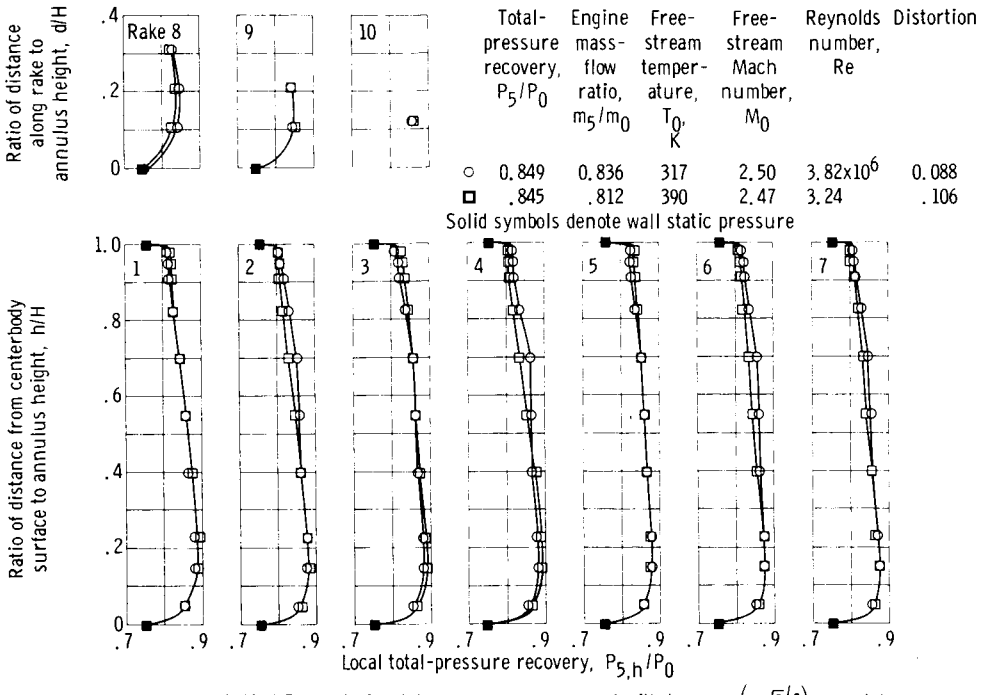

(f) 91.6 Percent of match pressure recovery set with bypass, $\left(w\sqrt{\theta}/\delta\right)_5$ = match.

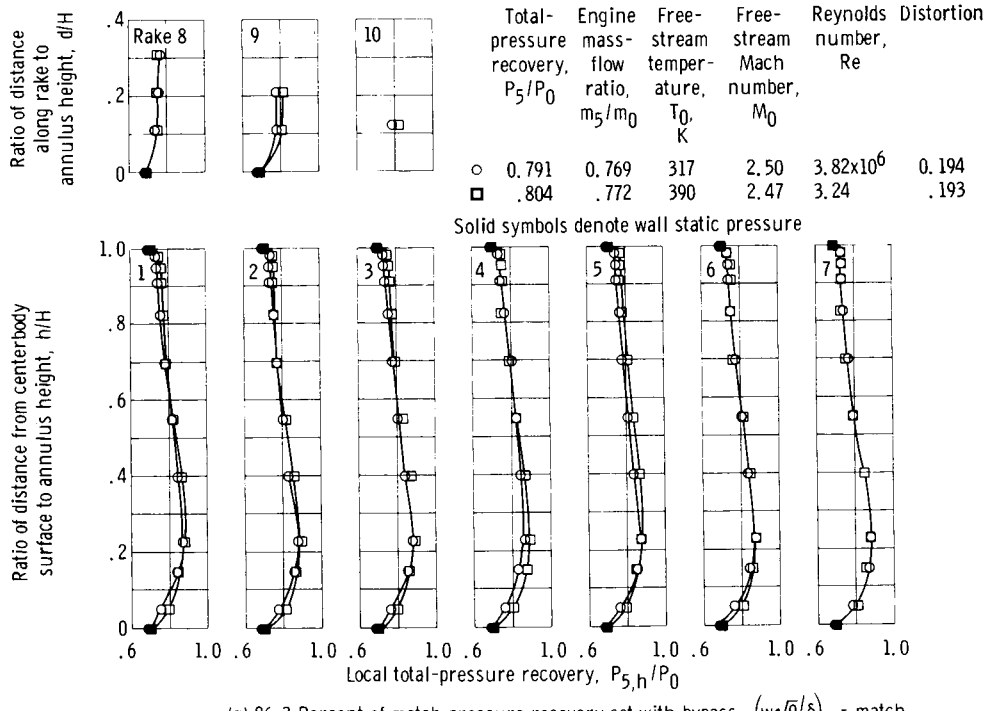

(g) 86.3 Percent of match pressure recovery set with bypass, $\left(w\sqrt{\theta}/\delta\right)_5$ = match.

Figure 11. - Concluded.

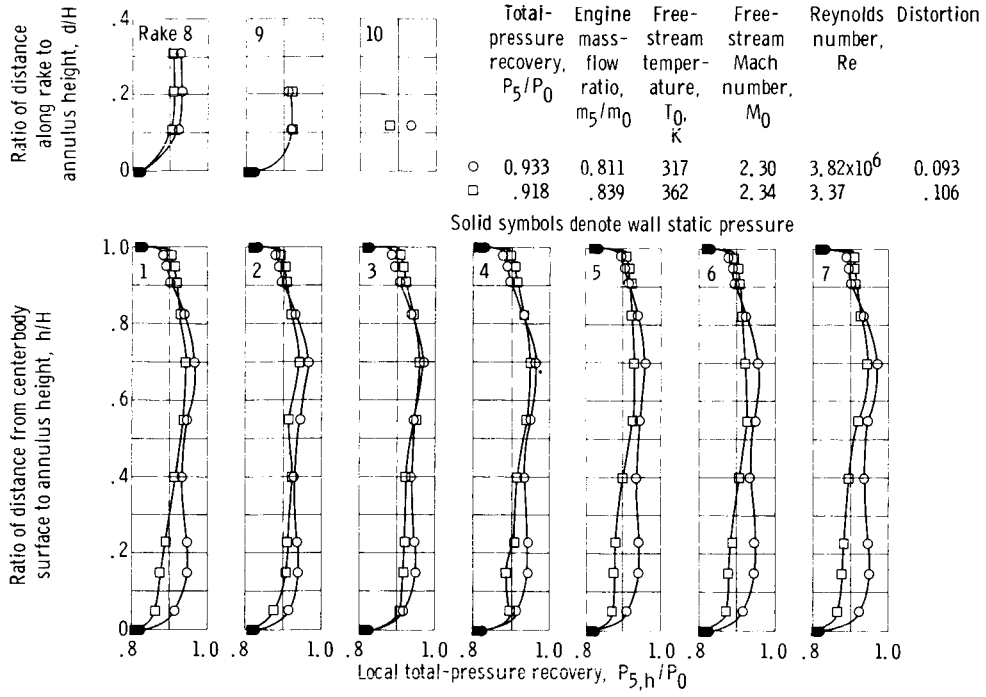

Figure 12. - Comparison of compressor-face total-pressure profiles at engine match conditions with and without tunnel heat. Configuration IIND'; nominal free-stream Mach number, 2.3; angle of attack, 0°; ejector area to capture area ratio, 0.0076.

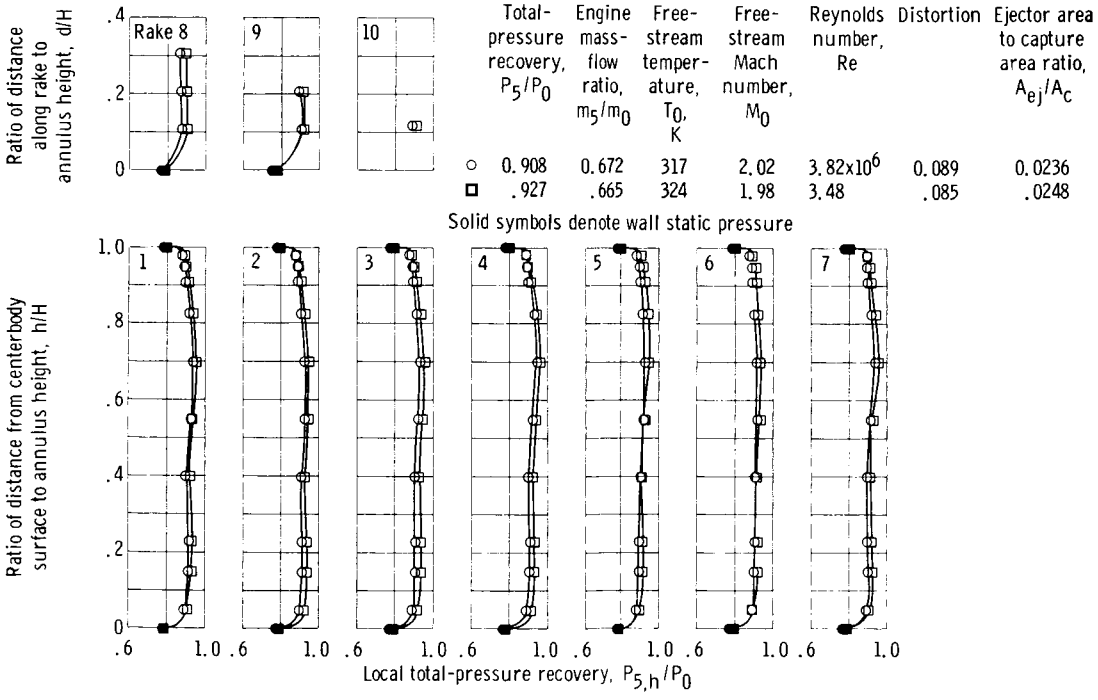

Figure 13. - Comparison of compressor-face total-pressure profiles at engine match conditions with and without tunnel heat. Configuration IIND'; nominal free-stream Mach number, 2.0; angle of attack, 0°.

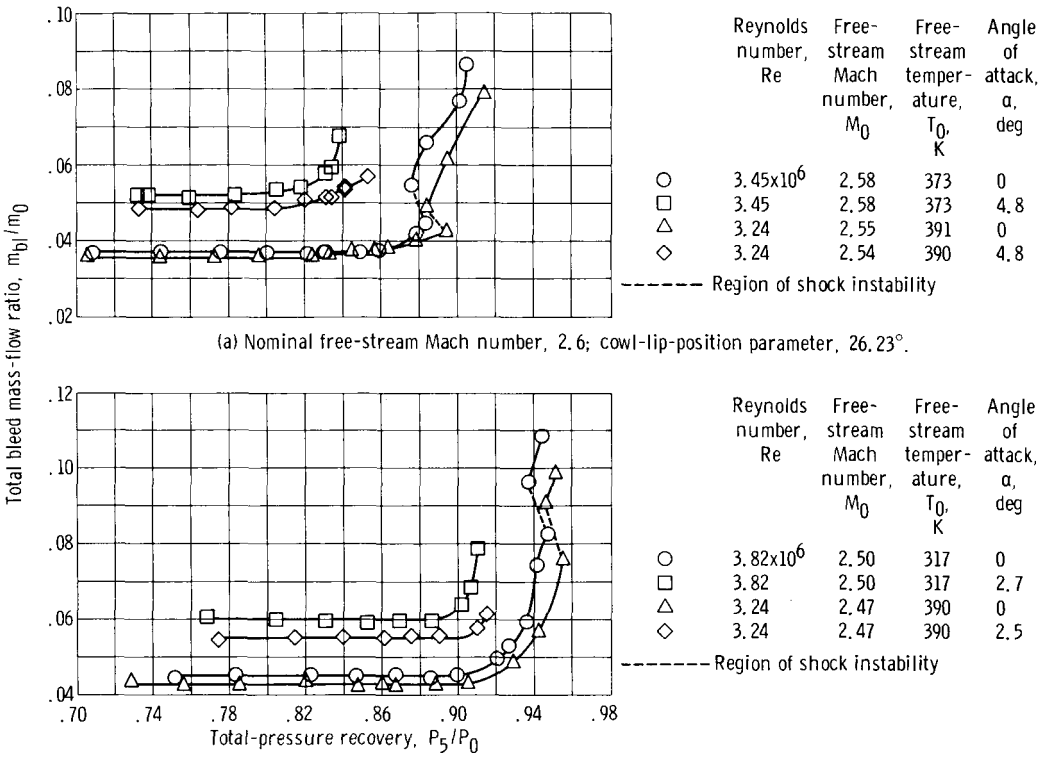

(a) Nominal free-stream Mach number, 2.6; cowl-lip-position parameter, 26.23°.

(b) Nominal free-stream Mach number, 2.5; cowl-lip-position parameter, 26.6°.

Figure 14. - Variation of bleed flow of inlet configuration IIND' with bypass flow.

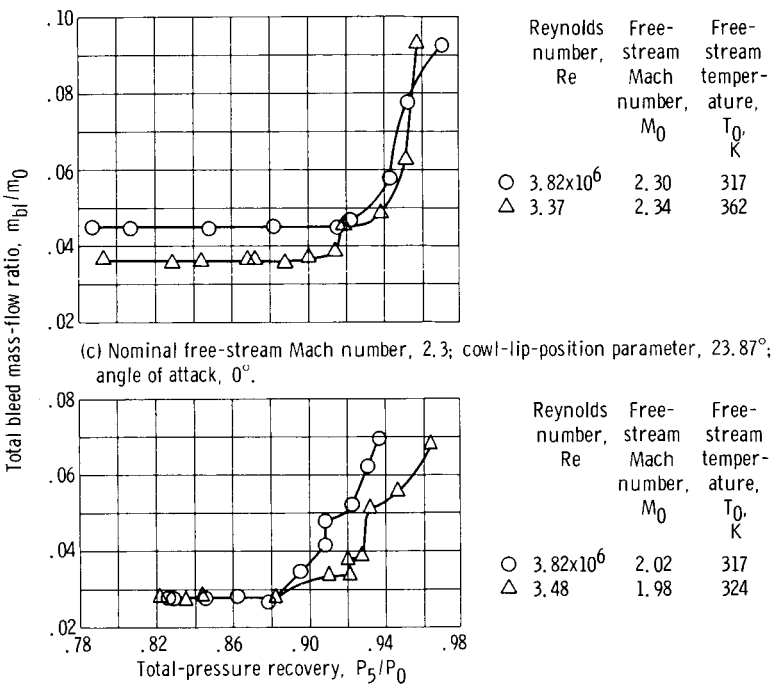

(c) Nominal free-stream Mach number, 2.3; cowl-lip-position parameter, 23.87°; angle of attack, 0°.

(d) Nominal free-stream Mach number, 2.0; cowl-lip-position parameter, 20.6°; angle of attack, 0°.

Figure 14. - Concluded.

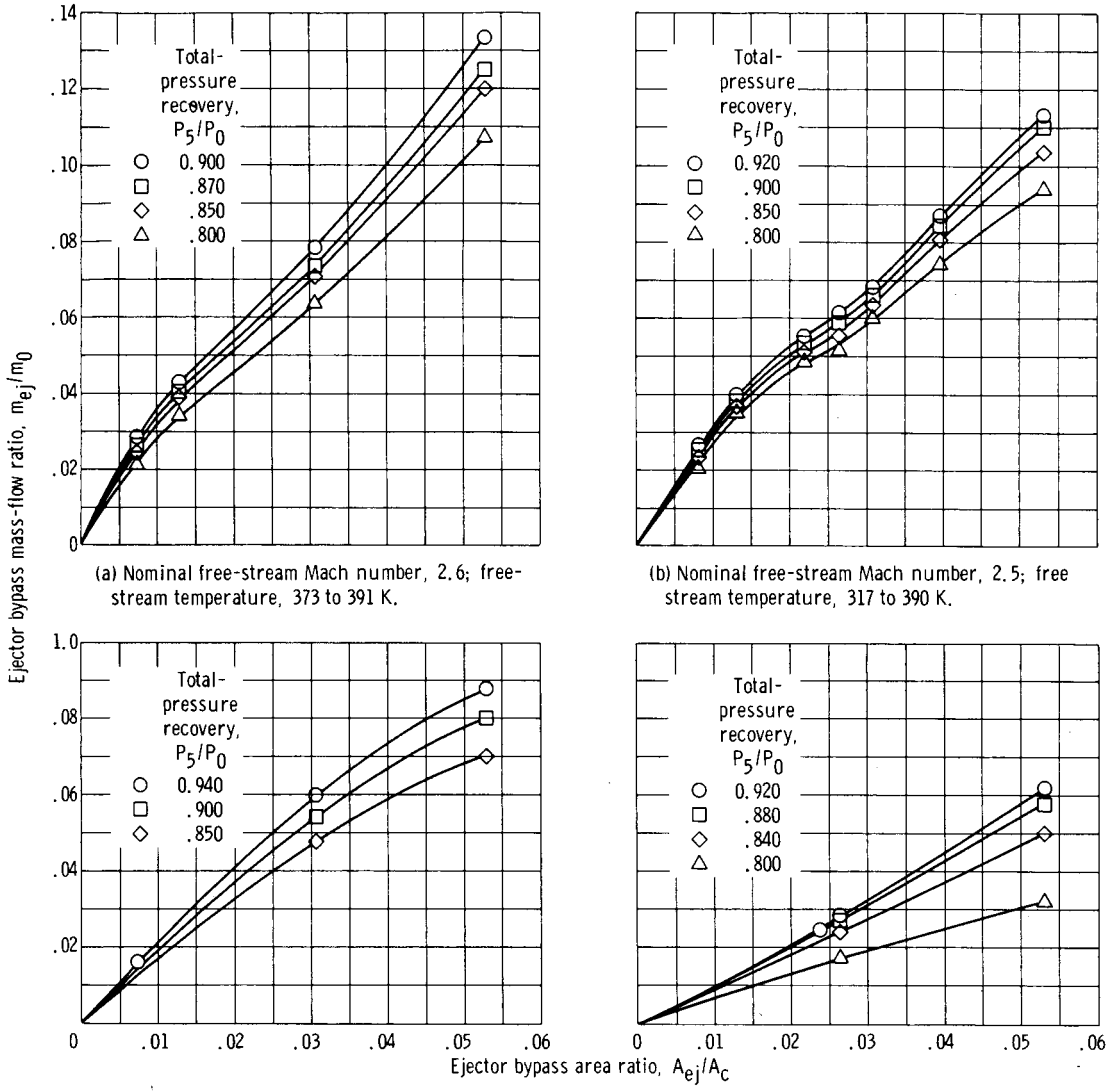

(a) Nominal free-stream Mach number, 2.6; free-stream temperature, 373 to 391 K.

(b) Nominal free-stream Mach number, 2.5; free stream temperature, 317 to 390 K.

(c) Nominal free-stream Mach number, 2.3; free-stream temperature, 317 to 362 K.

(d) Nominal free-stream Mach number, 2.0; free-stream temperature, 317 to 324 K.

Figure 15. - Ejector bypass operating characteristics.

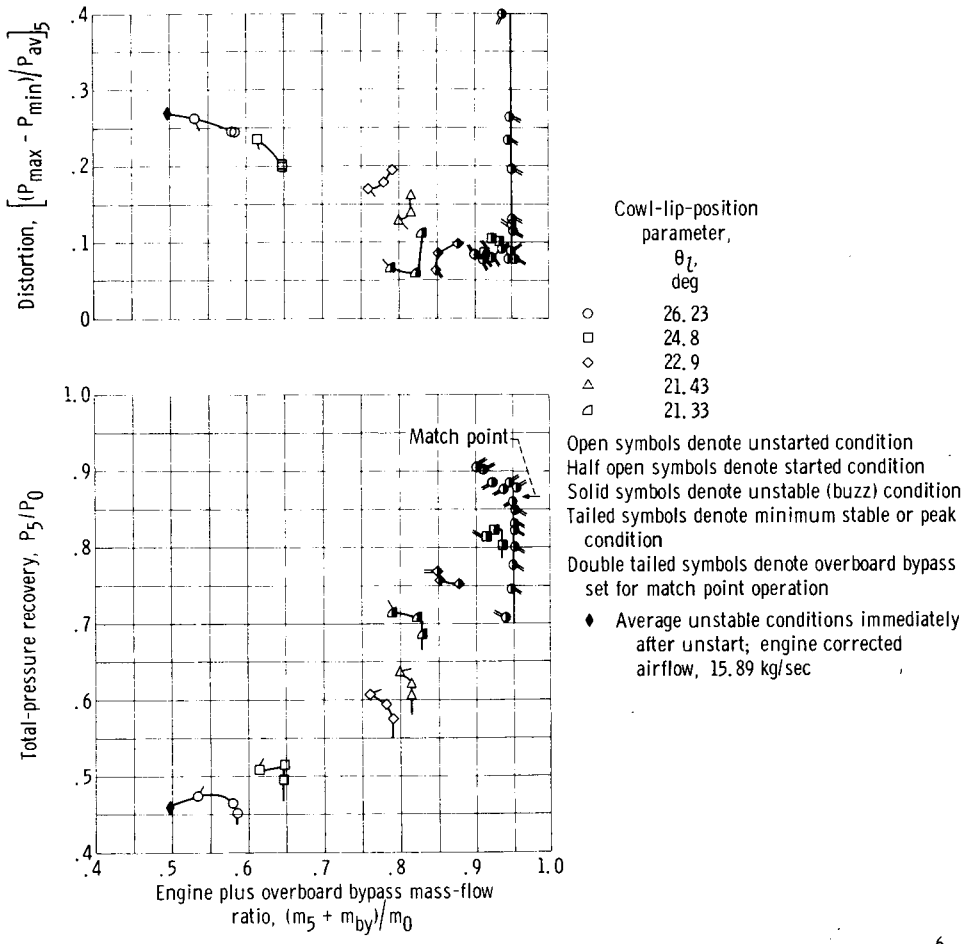

(a) Free-stream Mach number, 2.58; free-stream temperature, 373 K; Reynolds number, 3.45×10^6; ejector area to inlet capture area ratio, 0.0075.

Figure 16. - Overall inlet performance during restart sequence of configuration IIND'; angle of attack, 0°.

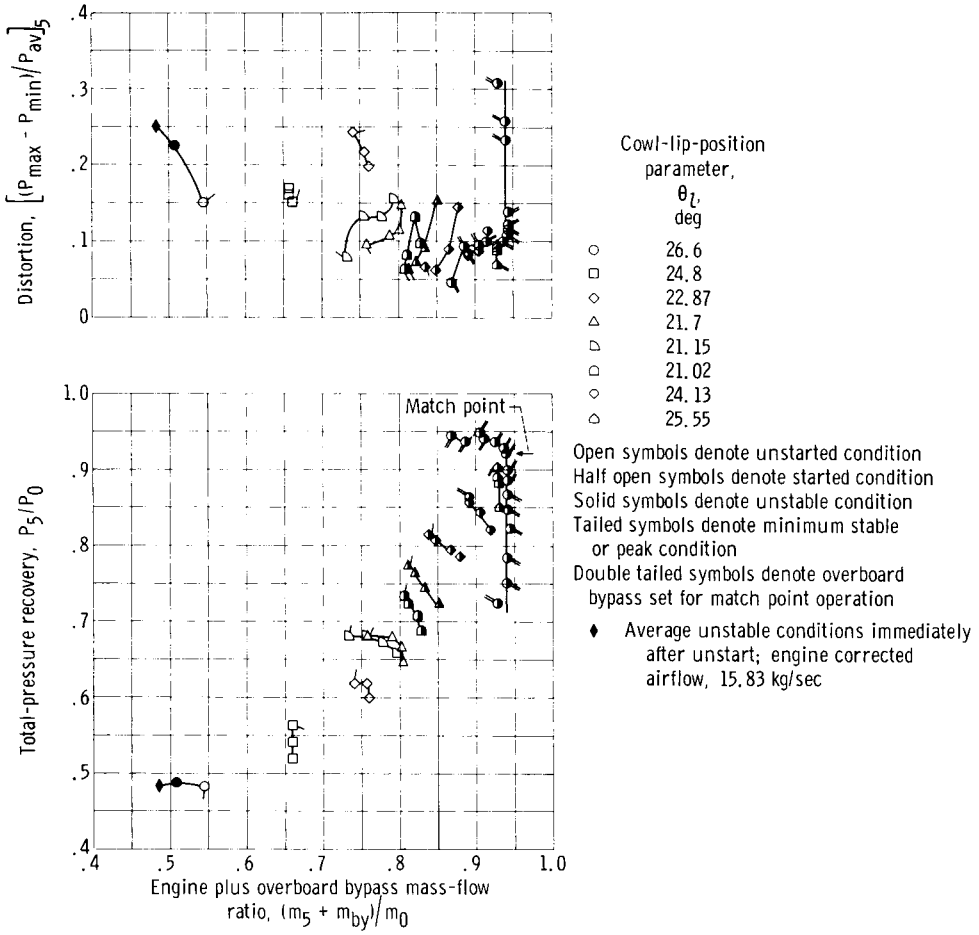

(b) Free-stream Mach number, 2.50; free-stream temperature, 317 K; Reynolds number, 3.82×10^6; ejector area to inlet capture area ratio, 0.0081.

Figure 16. - Continued.

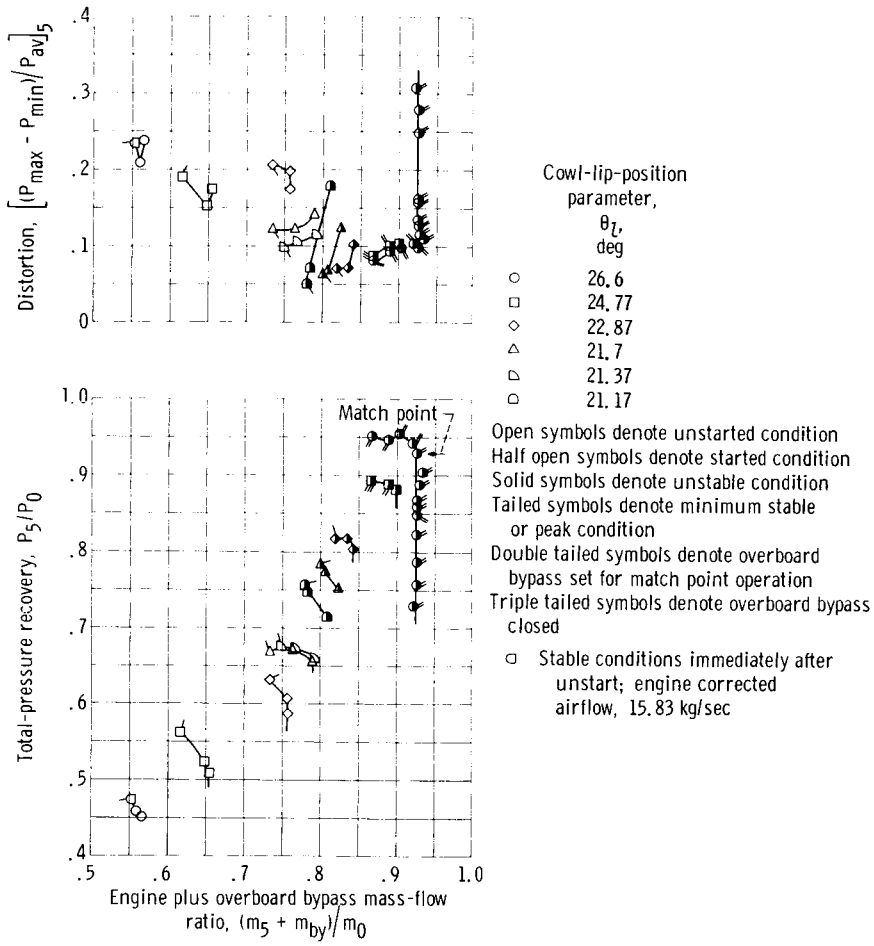

(c) Free-stream Mach number, 2.47; free-stream temperature, 390 K; Reynolds number, 3.24×10^6; ejector area to inlet capture area ratio, 0.0081.

Figure 16. - Continued.

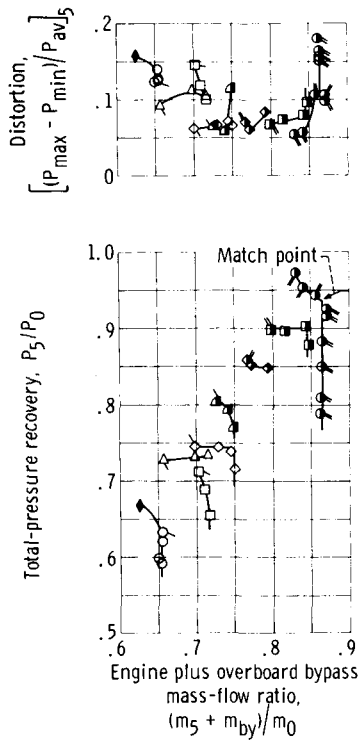

Cowl-lip-position parameter, θ_l, deg

○	23.87
□	22.6
◇	21.5
△	20.43
◻	20.25

Open symbols denote unstarted condition
Half open symbols denote started condition
Solid symbols denote unstable condition
Tailed symbols denote minimum stable or peak condition
Double tailed symbols denote overboard bypass set for match point operation

♦ Average unstable conditions immediately after unstart; engine corrected airflow, 16.75 kg/sec

(d) Free-stream Mach number, 2.30; free-stream temperature, 317 K; Reynolds number, 3.82×10^6; ejector area to inlet capture area ratio, 0.0076.

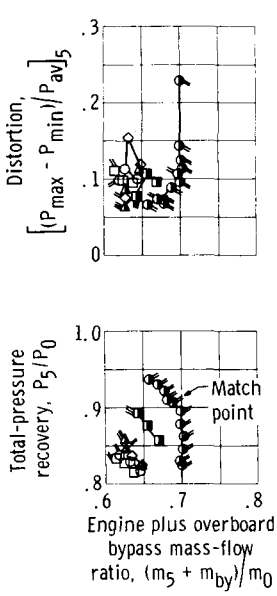

Cowl-lip-position parameter, θ_l, deg

○	20.6
□	19.95
◇	19.4
△	19.38

Open symbols denote unstarted condition
Half open symbols denote started condition
Solid symbols denote unstable condition
Tailed symbols denote minimum stable or peak condition
Double tailed symbols denote overboard bypass set for match point operation
Triple tailed symbols denote overboard bypass closed

◻ Stable conditions immediately after unstart; engine corrected airflow, 17.78 kg/sec

(e) Free-stream Mach number, 2.02; free-stream temperature, 317 K; Reynolds number, 3.82×10^6; ejector area to inlet capture area ratio, 0.0236.

Figure 16. - Concluded.

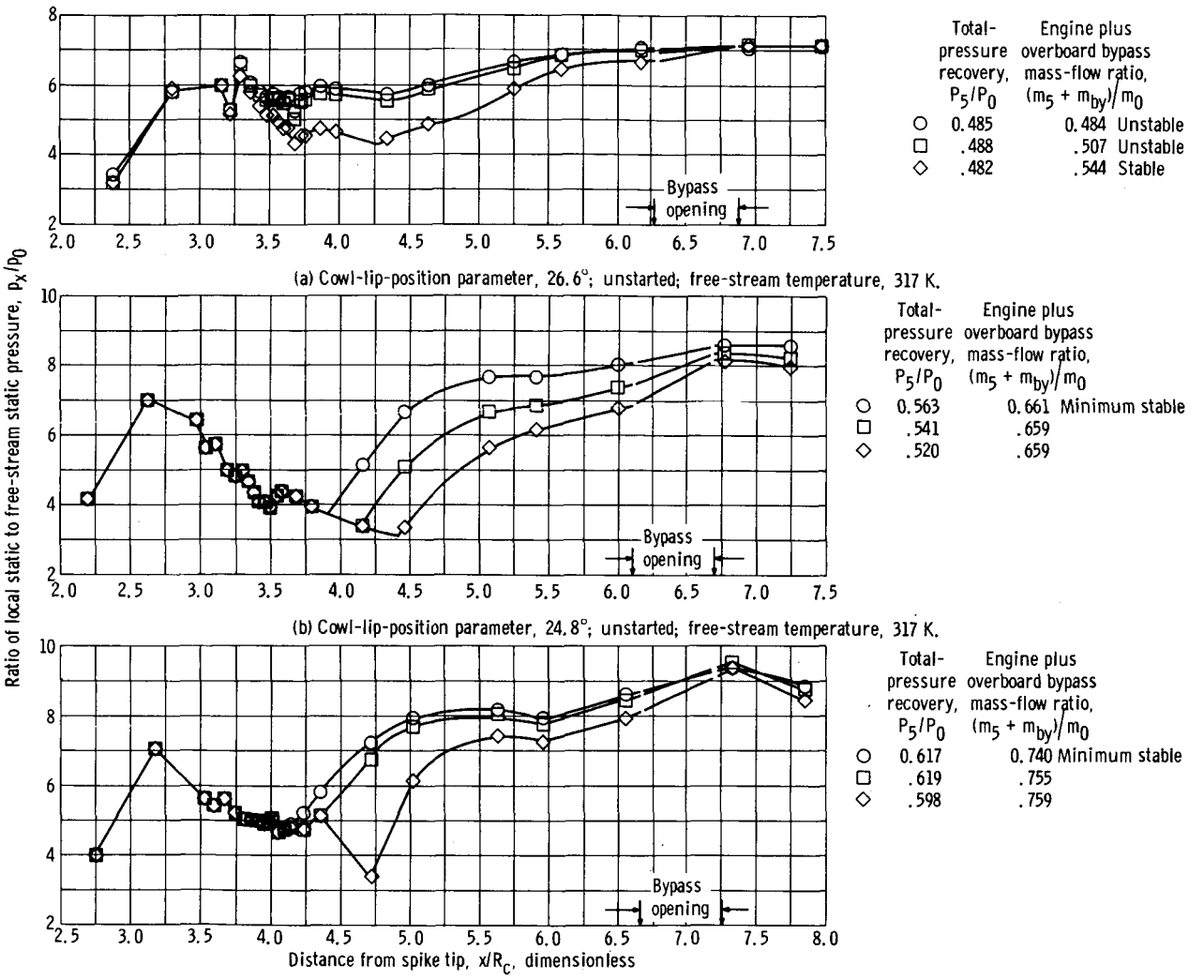

(c) Cowl-lip-position parameter, 22.87°; unstarted; free-stream temperature, 317 K.

Figure 17. - Internal cowl-surface static-pressure distributions during inlet restart sequence. Configuration IIND'; nominal free-stream Mach number, 2.5; Reynolds number, 3.82×10^6; angle of attack, 0°.

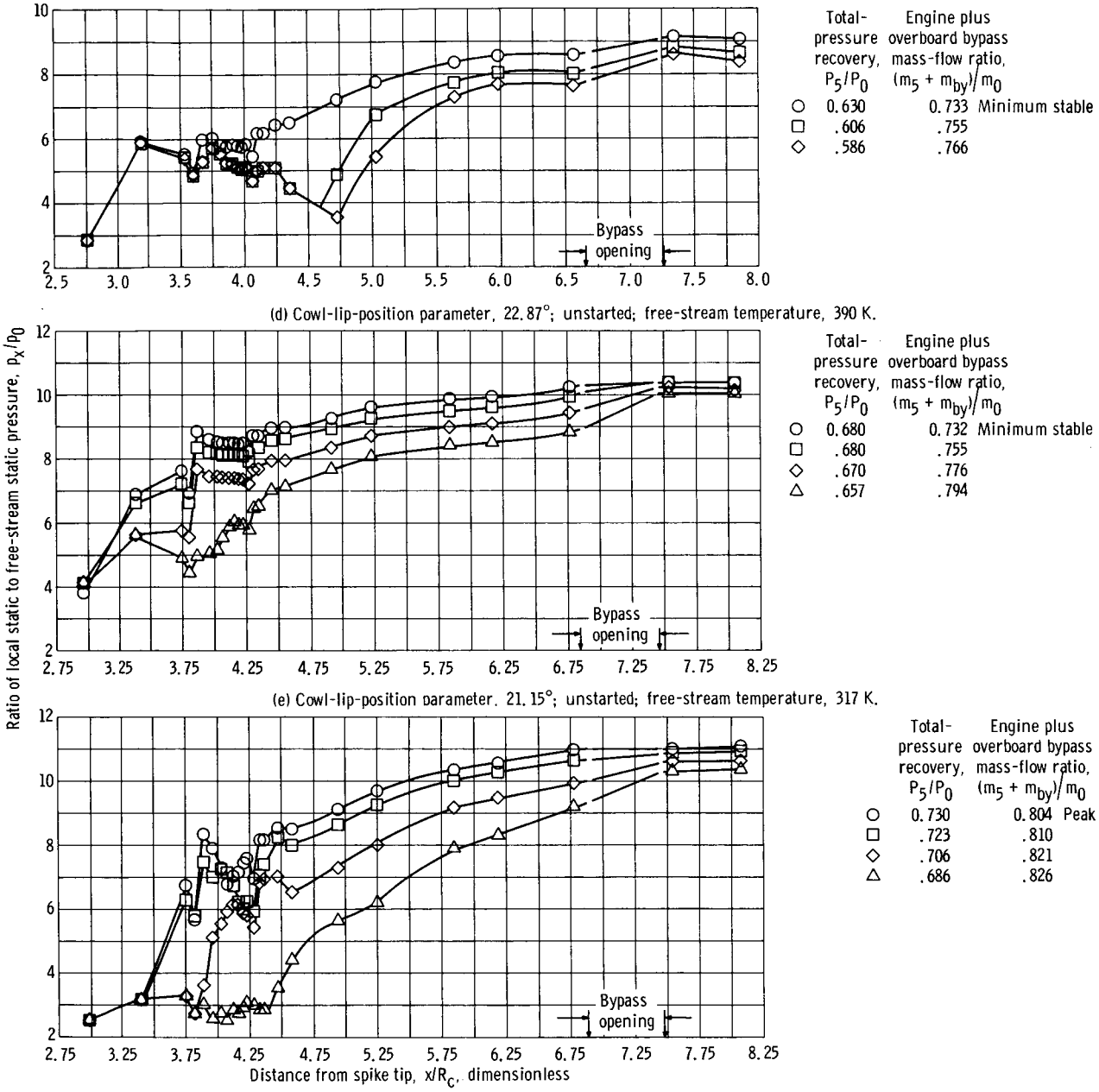

(d) Cowl-lip-position parameter, 22.87°; unstarted; free-stream temperature, 390 K.

(e) Cowl-lip-position parameter, 21.15°; unstarted; free-stream temperature, 317 K.

(f) Cowl-lip-position parameter, 21.02°; just started; free-stream temperature, 317 K.

Figure 17. - Continued.

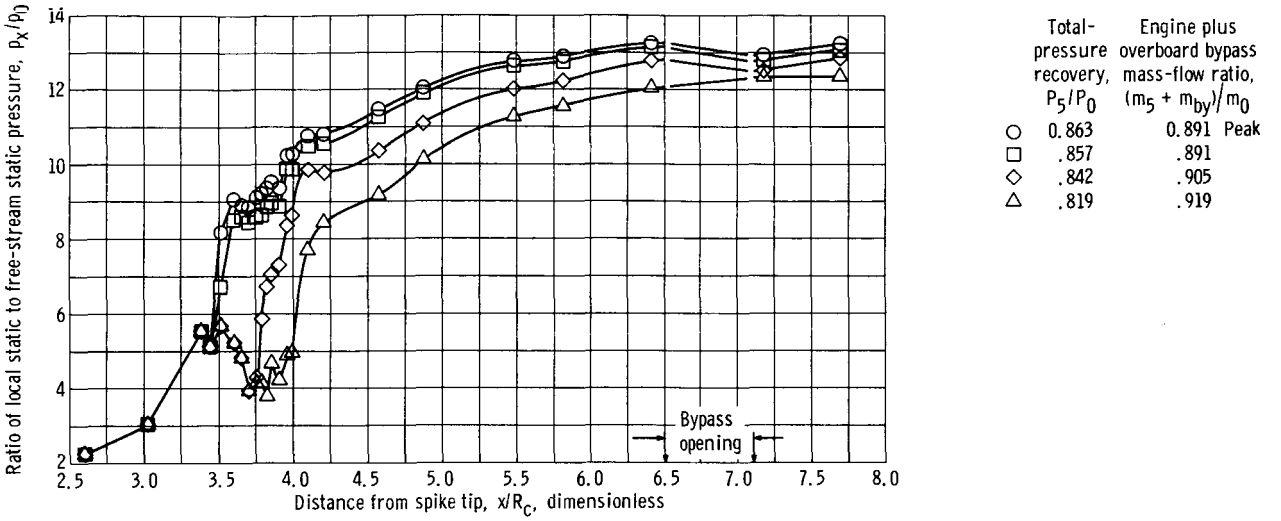

(g) Cowl-lip-position parameter, 24.13°; started; free-stream temperature, 317 K.

Figure 17. - Concluded.

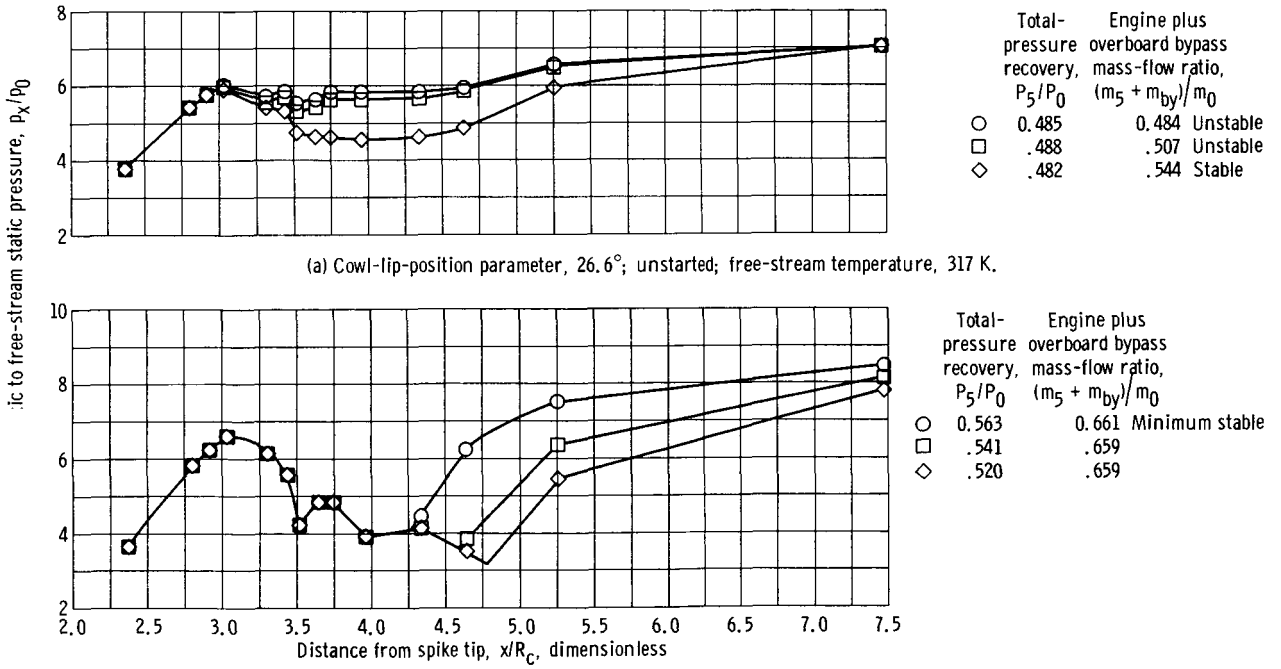

(a) Cowl-lip-position parameter, 26.6°; unstarted; free-stream temperature, 317 K.

(b) Cowl-lip-position parameter, 24.8°; unstarted; free-stream temperature, 317 K.

Figure 18. - Centerbody surface static-pressure distributions during inlet restart sequence. Configuration IIND'; nominal free-stream Mach number, 2.5; Reynolds number, 3.82×10^6; angle of attack, 0°.

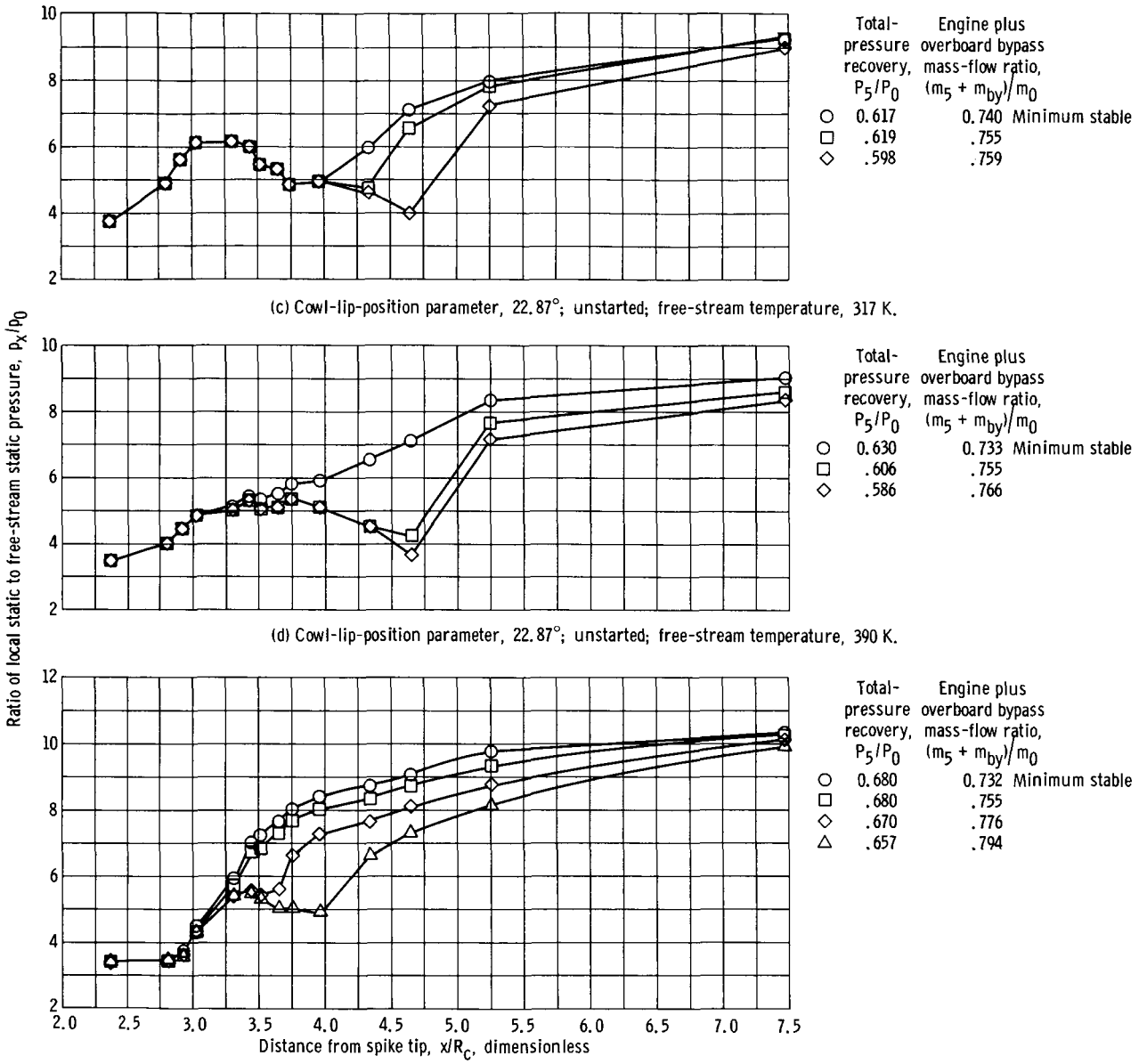

(c) Cowl-lip-position parameter, 22.87°; unstarted; free-stream temperature, 317 K.

(d) Cowl-lip-position parameter, 22.87°; unstarted; free-stream temperature, 390 K.

(e) Cowl-lip-position parameter, 21.15°; unstarted; free-stream temperature, 317 K.

Figure 18. - Continued.

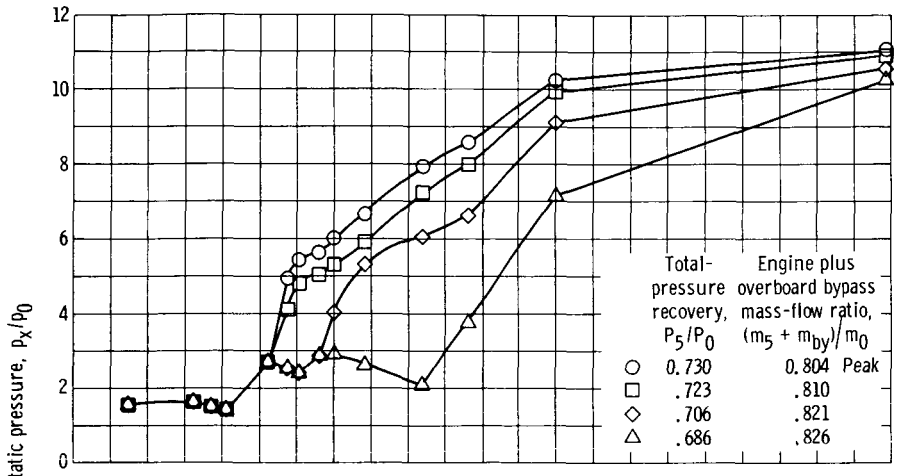

(f) Cowl-lip-position parameter, 21.02°; just started; free-stream temperature, 317 K.

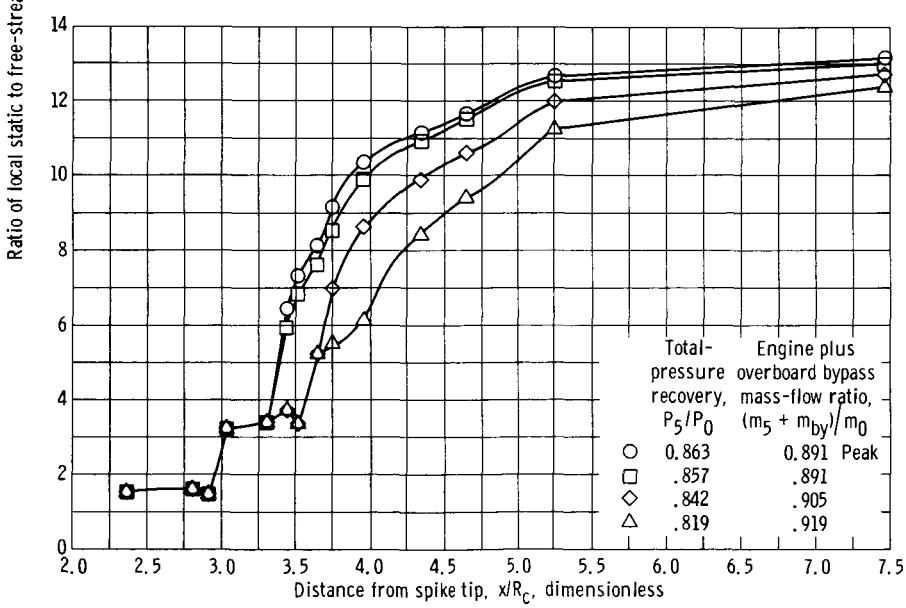

(g) Cowl-lip-position parameter, 24.13°; started; free-stream temperature, 317 K.

Figure 18. - Concluded.

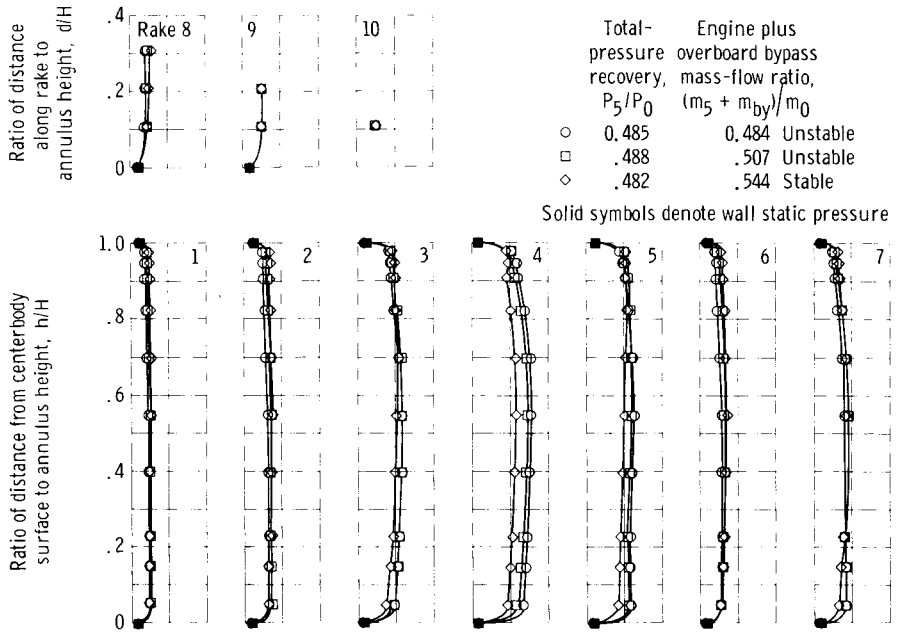

(a) Cowl-lip-position parameter, 26.6°; unstarted; free-stream temperature, 317 K.

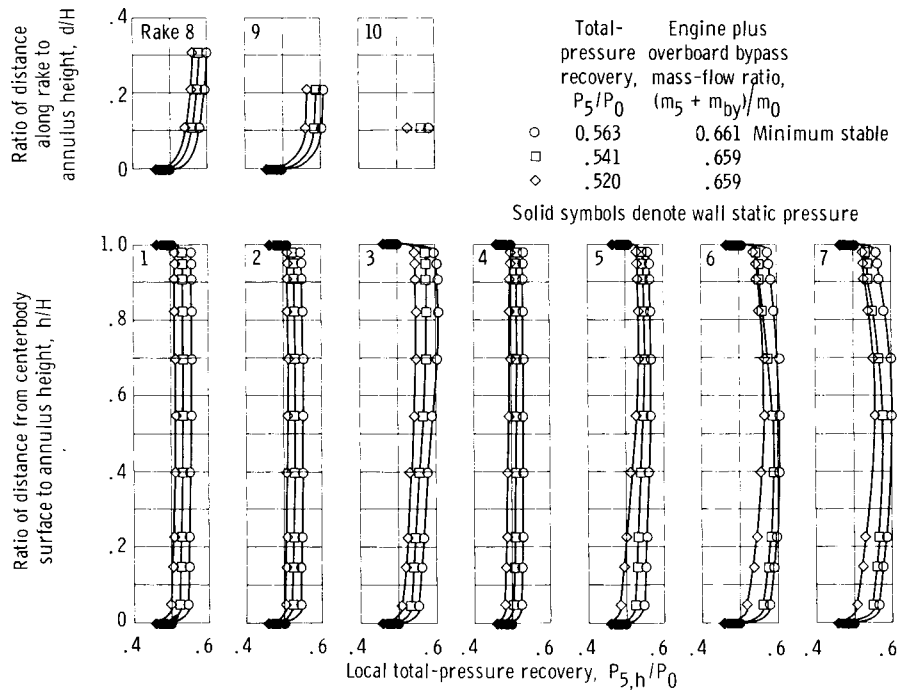

(b) Cowl-lip-position parameter, 24.8°; unstarted; free-stream temperature, 317 K.

Figure 19. - Comparison of compressor face total-pressure profiles during inlet restart sequence. Configuration IIND'; nominal free-stream Mach number, 2.50; Reynolds number, 3.82×10^6; angle of attack, 0°.

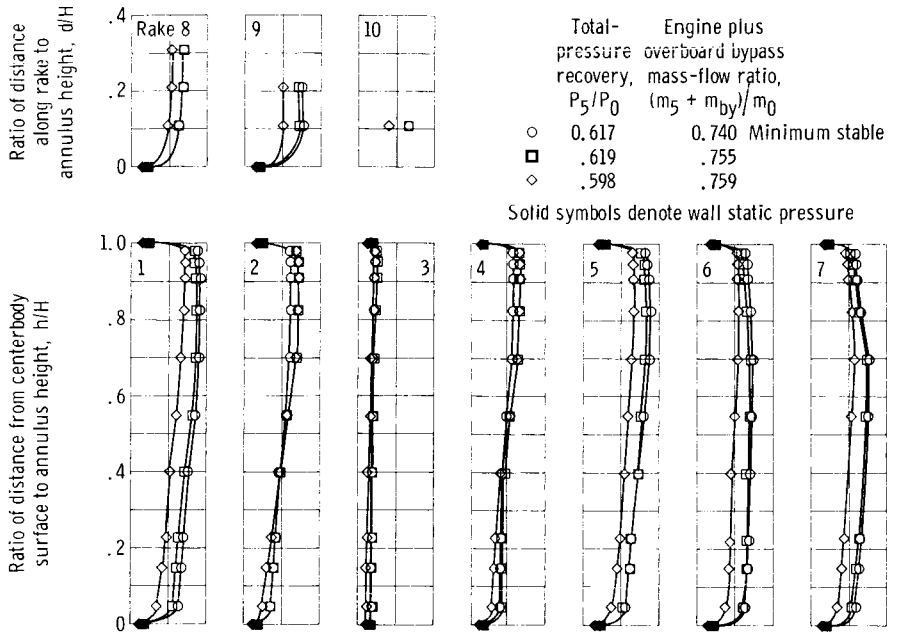

(c) Cowl-lip-position parameter, 22.87°; unstarted; free-stream temperature, 317 K.

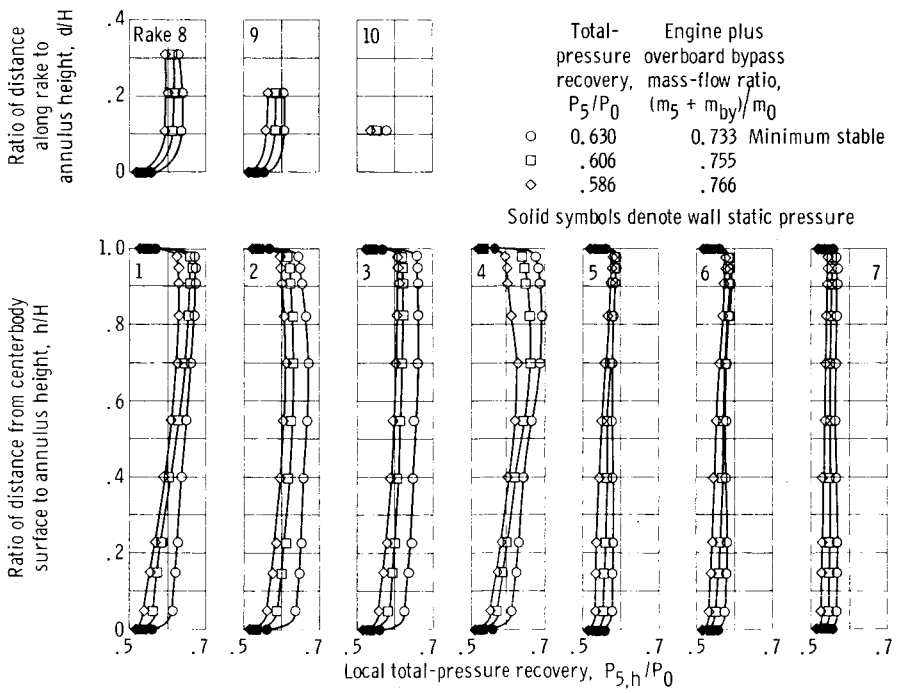

(d) Cowl-lip-position parameter, 22.87°; unstarted; free-stream temperature, 390 K.

Figure 19. - Continued.

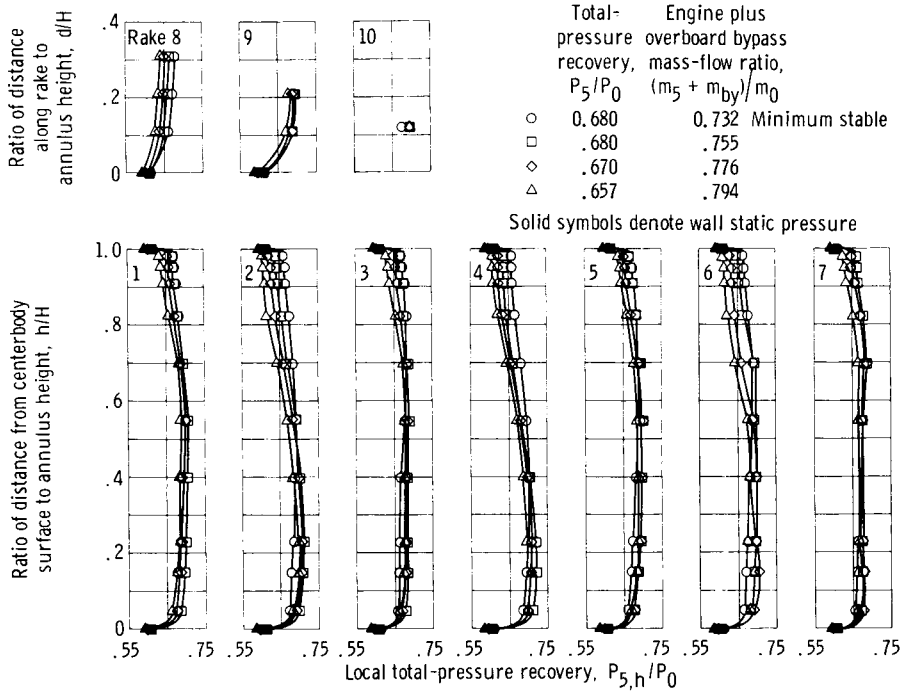

(e) Cowl-lip-position parameter, 21.15°; unstarted; free-stream temperature, 317 K.

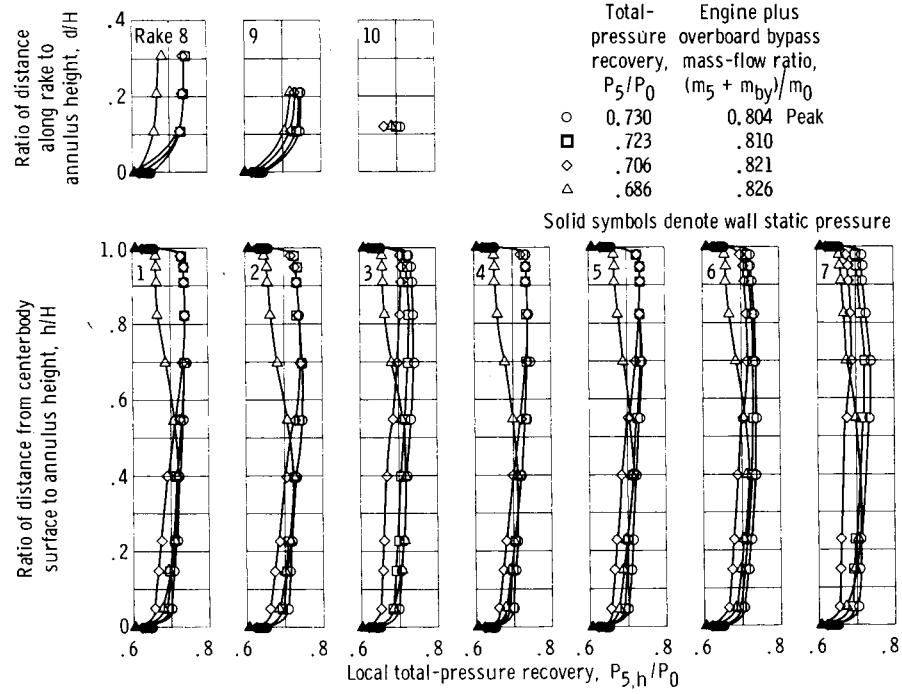

(f) Cowl-lip-position parameter, 21.02; just started; free-stream temperature, 317 K.

Figure 19. - Continued.

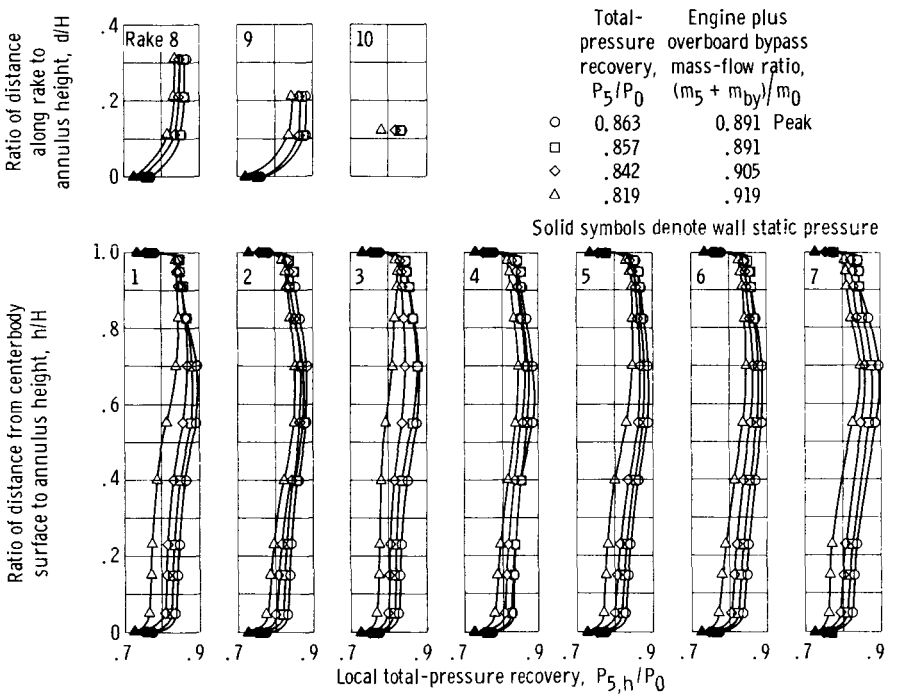

(g) Cowl-lip-position parameter, 24.13°; started; free-stream temperature, 317 K.

Figure 19. - Concluded.

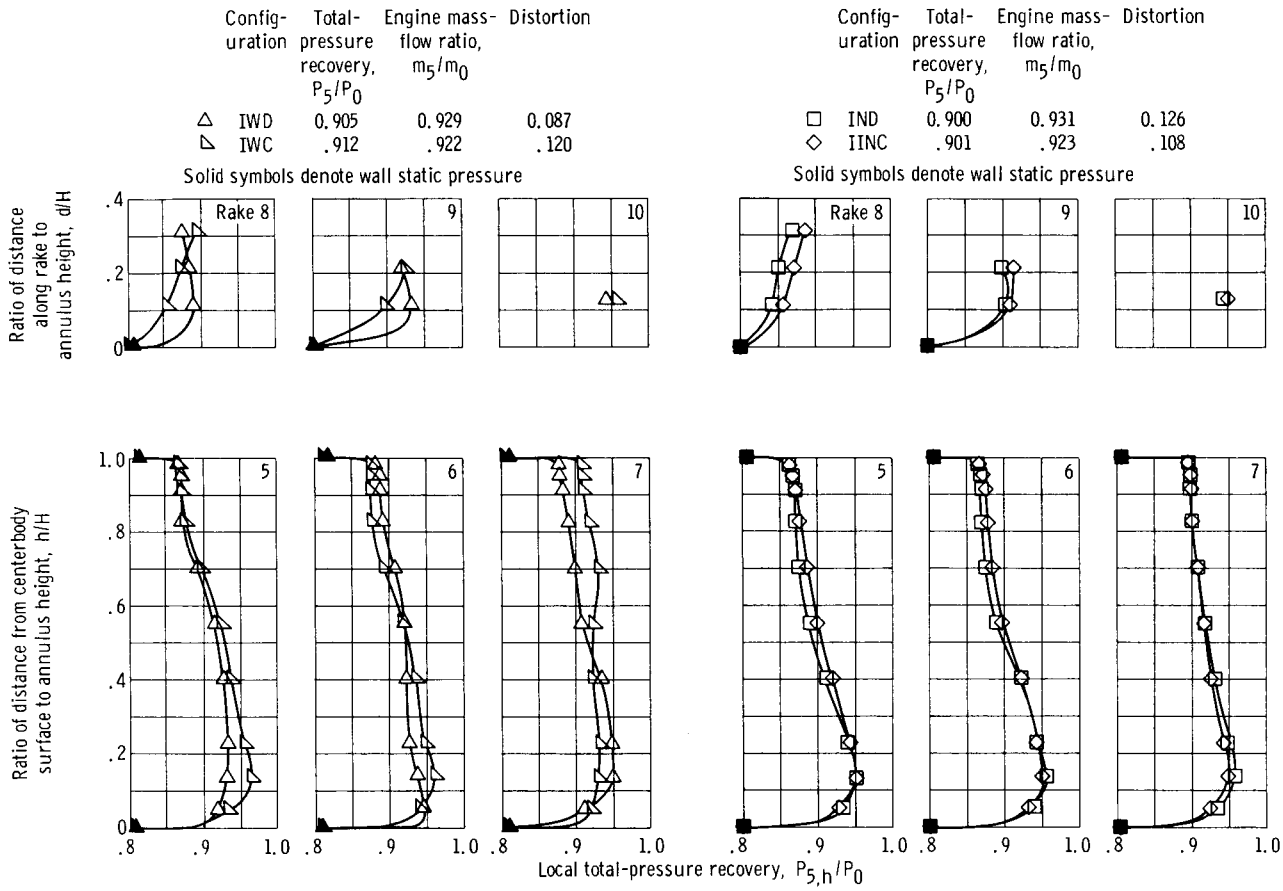

(a) Configurations IWC and IWD.

(b) Configurations IINC and IND.

Figure 20. - Effect of vortex generator orientation on engine-face total-pressure measurements. Free-stream Mach number, 2.50; angle of attack, 0°; no bypass; free-stream temperature, 317 K; Reynolds number, 3.82×10^6.

Configuration	○ I	□ IIND'	○ I	□ IIND'	○ I	□ IIND'	○ I	□ IIND'	○ I	□ IIND'	○ I	□ IIND'
Bypass mass-flow ratio, m_{by}/m_0	0	0	0.041	0.041	0.079	0.077	0.123	0.128	0.123	0.247	0.123	0.445
Total-pressure recovery, P_5/P_0	0.924	0.928	0.925	0.944	0.937	0.950	0.940	0.955	0.940	0.950	0.940	0.939
Distortion	0.115	0.079	0.106	0.055	0.099	0.063	0.101	0.058	0.101	0.046	0.101	0.052

Solid symbols denote wall static pressure

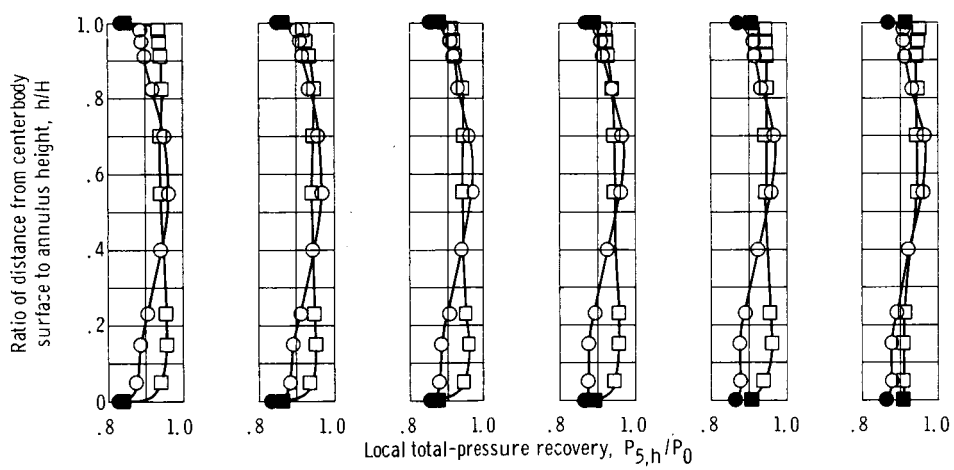

Figure 21. - Effect of centerbody vortex generators on engine face total-pressure profiles of rake 7 with bypass operation. Peak inlet operation; free-stream Mach number, 2.50; free-stream temperature, 317 K; angle of attack, 0°; Reynolds number, 3.82×10^6.

	Free-stream Mach number, M_0	Reynolds number, Re	Cowl-lip-position parameter, θ_l, deg	Free-stream temperature, T_0, K
○	2.58	3.45×10^6	26.23	373
□	2.50	3.82	26.6	317
◇	2.30	3.82	23.87	317
△	2.02	3.82	20.6	317

Solid symbols denote overboard bypass fully open

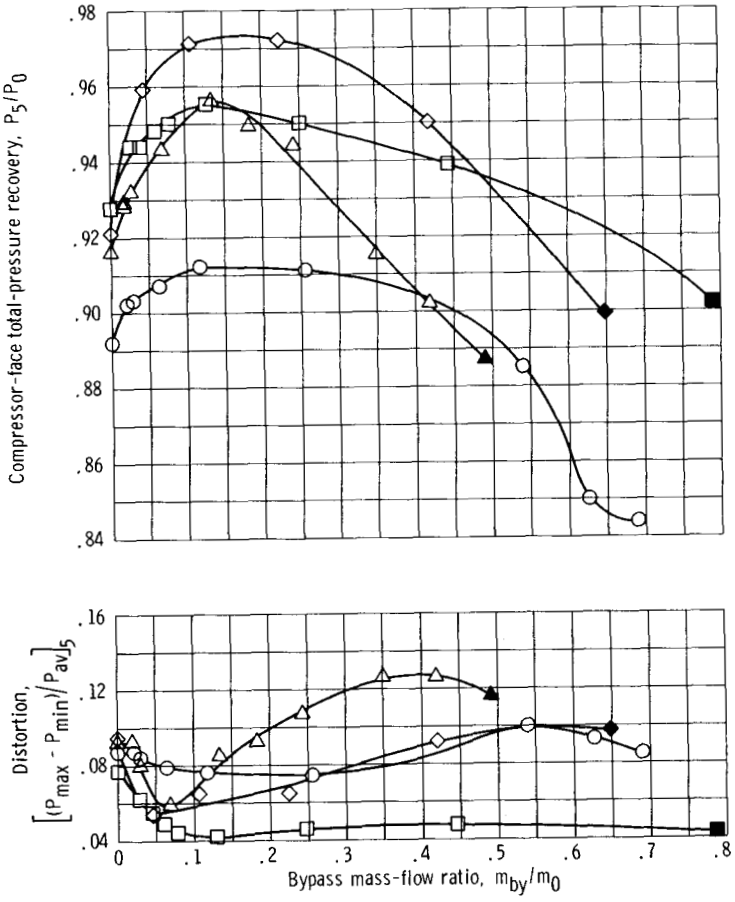

Figure 22. - Effect of bypass flow on peak inlet performance. Configuration IIND'; angle of attack, 0°.

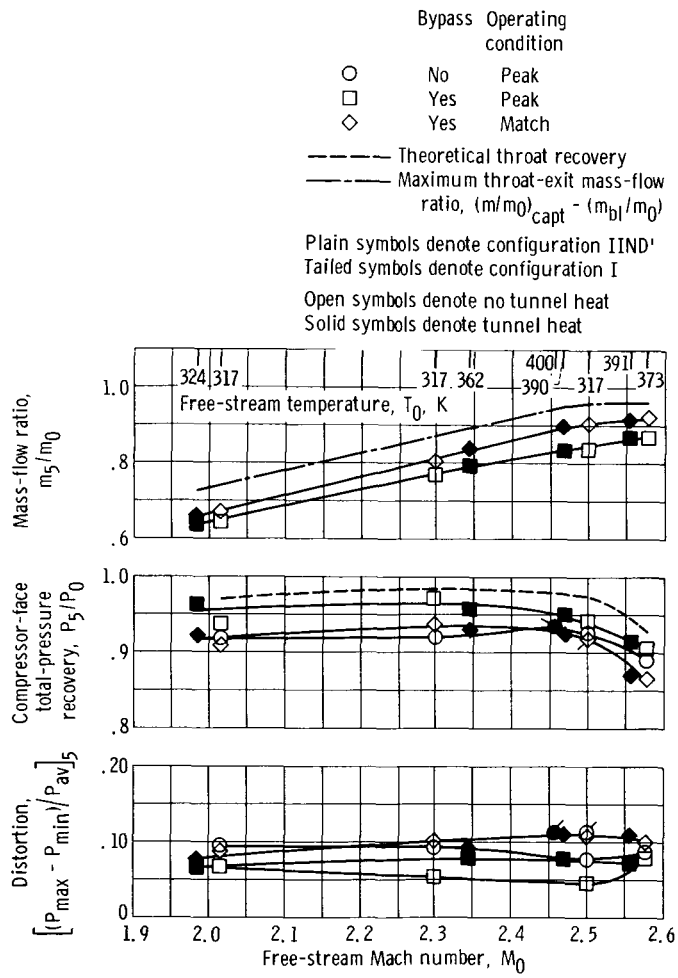

Figure 23. - Effect of Mach number on inlet performance parameters. Angle of attack, 0°.

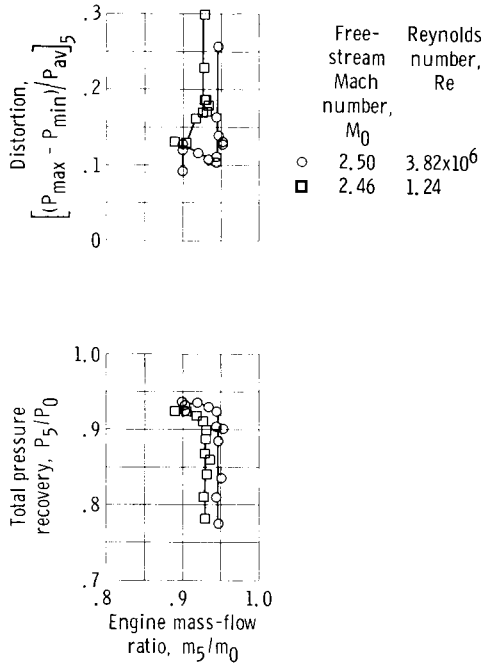

Figure 24. - Effect of Reynold's number on inlet performance without bypass. Centerbody vortex generators installed; configuration IIND'; free-stream temperature, 317 K; angle of attack, 0°; cowl-lip-position parameter, 26.6°.

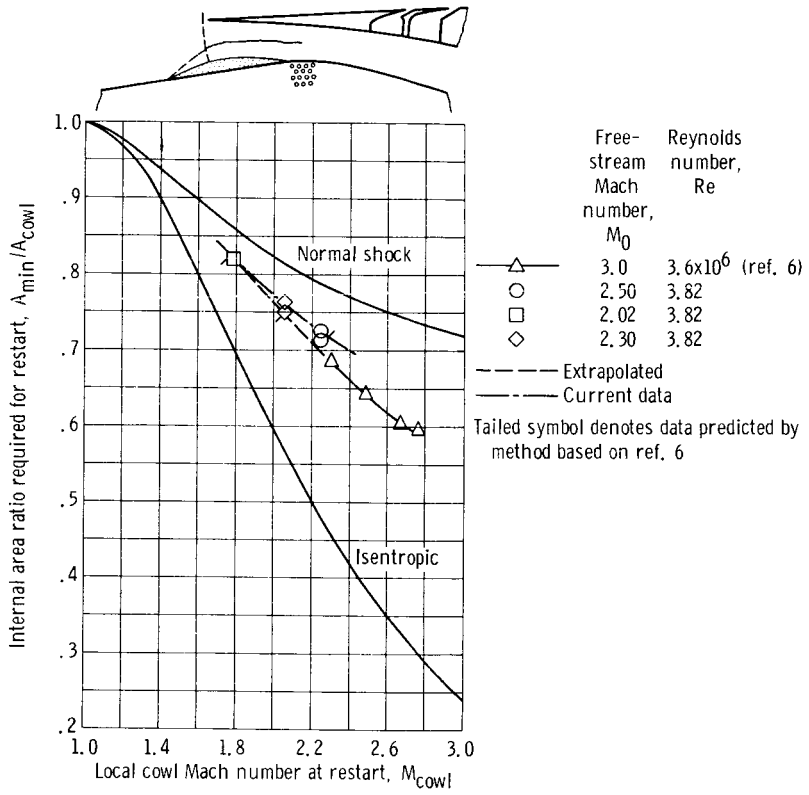

Figure 25. - Comparison of actual to predicted restart area ratio.